

**Asymmetric Chromosome Oscillation during Mitosis and Protein
Architecture of the Human Kinetochores Measured by K-SHREC
(Kinetochores-Speckle High Resolution Co-Localization)**

Xiaohu Wan

A dissertation submitted to the faculty of the University of North Carolina at
Chapel Hill in partial fulfillment of the requirements for the degree of Doctor of
Philosophy in the Department of Biomedical Engineering.

Chapel Hill
2008

Approve by:

Advisor: Professor E.D. Salmon, Ph.D.

Reader: Professor Henry Hsiao, Ph.D.

Reader: Professor Oleg Favorov, Ph.D.

Reader: Professor Kerry Bloom, Ph.D.

Reader: Professor Carol Lucas, Ph.D.

©2008
Xiaohu Wan
ALL RIGHTS RESERVED

ABSTRACT

XIAOHU WAN: Asymmetric Chromosome Oscillation during Mitosis and Protein Architecture of the Human Kinetochores Measured by K-SHREC (Kinetochores-Speckle High Resolution Co-Localization)

(Under the direction of Dr. E.D. Salmon)

Mitotic chromosomes are known to oscillate during prometaphase and metaphase. This study demonstrated that kinetochores move faster in poleward (P) motion than in away-from-the-pole (AP) motion. P and AP motions also showed different position versus time curves, suggesting distinct mechanisms behind the phenomenon. Sister kinetochores oscillate with different phases relative to each other. The leading kinetochore usually switches first, from P to AP motion, followed by the trailing one switching from AP to P motion. Such asymmetry and phase lag produces oscillation in centromere stretch at twice the frequency of individual kinetochores. The leading kinetochore switches after sister chromosomes reach maximum centromere stretch, suggesting tension may trigger the kinetochore switching.

To further investigate kinetochore dynamics, K-SHREC (Kinetochores-Speckle High Resolution Co-Localization) was developed to map the relative protein positions within kinetochores using two color fluorescent speckle microscopy, where centroids, orientations and geometries of fluorescent proteins were identified by asymmetric 3D Gaussian fitting in 3D image stacks. The accuracy of this method can reach ± 5 nm. The

relative positions of kinetochore proteins such as CenpA, Spc24, Spc25, Bub1, DC31, KNL1 and KNL3 to another kinetochore protein Hec1 were assessed in fixed HeLa cells at metaphase. When centromeric tension is lost by taxol treatment, Ndc80 complex remains the same orientation and fully extended with 45nm-separation between the N-termini of Hec1 and Spc24. Most proteins moved about 30 nm closer to CENP-A, except Bub1. This result suggests that there is a tension-sensitive linkage between the KNL-1/Mis12 complex/Ndc80 complex (KMN) network of proteins in the core microtubule attachment site and the location of the majority of CENP-A within the peripheral centromere. The Ndc80 complex behaves like a stiff object, perhaps a thin rod.

The relative positions between the end of kinetochore microtubule and the centroid of the fluorescent speckle of Hec1 were also measured by imaging GFP-tubulin. A 3D line scan method and an error function fitting algorithm were developed to identify the microtubule end position. Microtubule end stays closer to centromere with about 63nm distance from Hec1.

ACKNOWLEDGEMENTS

I thank Dr. Ted Salmon for his advice and guidance. I would also like to thank everyone who helped me during my graduate study. I am most grateful to my family for their support.

TABLE OF CONTENTS

LIST OF FIGURES	viii
LIST OF TABLES	xi
LIST OF ABBREVIATIONS.....	xii
CHAPTER 1: INTRODUCTION	1
Cell cycle and mitosis	1
Basic spindle structure in metaphase	2
Structure of kinetochore.....	3
Dissertation layout	4
CHAPTER 2: KINETOCHORE DETECTION	5
Image of kinetochore	5
Methods.....	6
CHAPTER 3: ACCURATE MEASUREMENT OF KINETOCHORE POSITION	10
Light microscopy	10
Two-dimensional Gaussian function	11
Least-square curve fitting	13
Three-dimensional Gaussian fitting.....	15
CHAPTER 4: KINETOCHORE TRACKING	16
Introduction.....	16
Methods.....	17

Results.....	24
Discussions	28
CHAPTER 5: CHROMOSOME DYNAMICS IN METAPHASE	30
Abstract.....	30
Methods.....	31
Results.....	32
Acknowledgements.....	45
CHAPTER 6: K-SHREC	46
Introduction.....	46
Methods.....	47
Results.....	64
Acknowledgements.....	81
CHAPTER 7: SOFTWARE DEVELOPMENT	83
Introduction.....	83
Software design.....	84
Software functions and instructions.....	85
REFERENCES	102

LIST OF FIGURES

Figure 1.1: Spindle structure.....	3
Figure 1.2: Kinetochore proteins	4
Figure 2.1: Image of kinetochores	5
Figure 2.2: Intensity levels of kinetochore and noise	6
Figure 2.3: Gaussian mask.....	8
Figure 2.4 Intensity levels of kinetochore and noise after mask operation	9
Figure 3.1: Image of PSF	11
Figure 4.1: Points from different frames.....	17
Figure 4.2: Point tracking	17
Figure 4.3: Nearest neighbor method.....	18
Figure 4.4: Limit of nearest neighbor method	19
Figure 4.5: Minimum square distance method	20
Figure 4.6: Kinetochore movement vectors.....	21
Figure 4.7: Tracking problem: point missing	23
Figure 4.8: Tracking problem: point emerging.....	23
Figure 4.9: Tracking problem: points overlapping	24
Figure 4.10: Good tracking results	26
Figure 4.11: Bad tracking results I	27
Figure 4.12: Bad tracking results II	28
Figure 5.1: Measured and labeled kinetochores	31
Figure 5.2: Distance between kinetochore and pole and distance between sister kinetochores	32

Figure 5.3: Oscillation frequencies	33
Figure 5.4: Oscillation models	34
Figure 5.5: Histogram of time difference between leading KT switching and trailing KT switching	37
Figure 5.6: Histogram of time difference between leading KT switching and max K-K distance	38
Figure 5.7: Histogram of time difference between trailing KT switching and max K-K distance	39
Figure 5.8: P kinetic curve	41
Figure 5.9: AP kinetic curve	41
Figure 5.10: P and AP kinetic curves.....	42
Figure 5.11: P and AP velocity curves	43
Figure 5.12: P and AP movements of monopole spindle.....	44
Figure 5.13: Velocities of monopole spindle.....	45
Figure 6.1: K-SHREC principles	48
Figure 6.2: Intensity level of kinetochore	51
Figure 6.3: Tilt of the kinetochore	53
Figure 6.4: Tilt correction for taxol data.....	57
Figure 6.5: Control results	58
Figure 6.6: Taxol results	59
Figure 6.7: Tilt correction for control data	60
Figure 6.8: Statistical test.....	61
Figure 6.9: MT end measurement.....	63
Figure 6.10: Compliance.....	67
Figure 6.11: Protein map.....	69

Figure 6.12: Control and taxol results.....	70
Figure 6.13: Kinetochores from nocodazole treated cells.....	79
Figure 6.14: Curvature of kinetochores.....	79
Figure 6.15: Simulated kinetochores images.....	80
Figure 6.16: Curvature and Delta.....	81
Figure 7.1 SpeckleTracker.....	83
Figure 7.2: Interface design.....	85
Figure 7.3: Open image.....	86
Figure 7.4: Image display.....	87
Figure 7.6: Zoom.....	89
Figure 7.7: Change label.....	90
Figure 7.8: Mask detector.....	91
Figure 7.9: Detect kinetochores.....	92
Figure 7.10: Gaussian fitting.....	93
Figure 7.11: Tracking.....	96
Figure 7.12: Input scale factor.....	97
Figure 7.13: Save labels.....	98
Figure 7.14: Plot kinetochores position.....	99
Figure 7.15: Distance between kinetochores and equator.....	99
Figure 7.16: Distance between kinetochores and pole.....	101

LIST OF TABLES

Table 2.1: Mask array	7
Table 2.2: Gaussian mask array	8
Table 4.1: List of all possible matches.....	20
Table 4.2: Tracking results of image sequence 1.....	25
Table 4.3: Tracking results of image sequence 2.....	25
Table 4.4: Tracking results of image sequence 3.....	26
Table 5.1: P and AP velocities and periods	35
Table 5.2: Monopole velocities and periods.....	45
Table 6.1: List of measurements.....	56
Table 6.2: Nocodazole measurements	81

LIST OF ABBREVIATIONS

AP – away-from-the-pole

GUI - graphical user interface

KT – kinetochore

kMT – kinetochore microtubule

K-SHREC – Kinetochore-Speckle High Resolution Co-Localization

MT – microtubule

K-K – kinetochore to kinetochore

K-P – kinetochore to pole

P – poleward

PSF – Point Spread Function

SNR – signal to noise ratio

CHAPTER 1

INTRODUCTION

During mitosis a cell divides itself into two daughter cells and identical genetic material (DNA) is distributed. Understanding the dynamics of cell division and its related structure is crucial to the study of mitosis, which is one of the fundamental functions of the cell. My research is focused on applying quantitative imaging approaches to assess such biological phenomenon, specifically studying the localization and colocalization, in sub-diffraction-limit precision, of kinetochore proteins related to cell division, as well as the dynamics of chromosome movement during mitosis.

Cell cycle and mitosis

There are four phases during a cell cycle: G1, S, G2 and M phases. G1, S and G2 are collectively called interphase. During the interphase a cell prepares itself for the subsequent cell division: its size grows and its DNA is replicated. In M phase (mitotic phase), the last phase of the cell cycle, a cell finishes its division. There are six stages in M phase: interphase, prophase, prometaphase, metaphase, anaphase, telophase.

Two daughter centrosomes separate and move to the opposite poles when cell enters into prophase. Microtubules are polymerized and projected from the poles and form the mitotic spindle in prophase. The breakdown of nuclear envelop indicates the onset of

prometaphase. Microtubules will then be able to connect with chromosomes at a specific site on the chromosome called the kinetochore. In metaphase, chromosome pairs are aligned across the spindle equator by microtubules with sister kinetochores attached to the opposite poles. When the cell enters into anaphase, its sister chromosomes separate and move to the poles.

This study focused on metaphase, in which chromosomes exhibit oscillation movement across spindle equator.

Basic spindle structure in metaphase

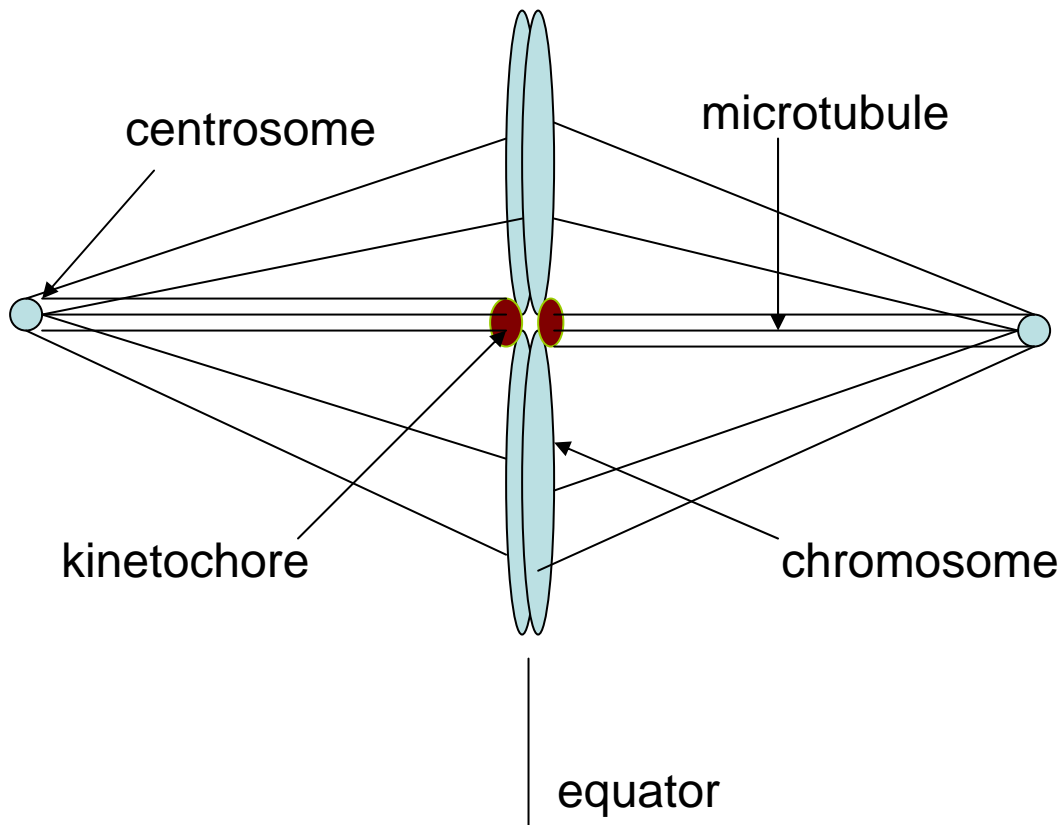


Figure 1.1: Spindle structure

A spindle is formed at the beginning of M phase (Figure 1.1). Spindle poles consist of a pair of centrosomes. Microtubules are emanated from the centrosome and connect chromosome at the kinetochore. During mitosis the spindle mechanism aligns the chromosomes at the center of the spindles in prometaphase and then separates the sister chromosomes to the opposite poles in anaphase.

The chromosomes are highly dynamic during mitosis. Chromosome movement is mediated by the force generated between microtubules and kinetochores, the tension between sister kinetochores, the force at the spindle pole, as well as microtubule assembly dynamics. Chromosomes move back and forth across the spindle equator during metaphase. The exact mechanism of the chromosome movement is still unknown.

Structure of kinetochore

Kinetochore contains many proteins and protein complexes (Figure 1.2, Musacchio and Salmon, 2007). It plays a crucial role in mitosis. It's widely accepted that kinetochore has an inner plate and outer plate. But exact locations of the kinetochore proteins and protein complexes are mostly unknown. Because the size of the kinetochore is small, less than the resolution limit of light microscope, it is impossible to directly resolve the detail structure of kinetochore using light microscopy. A technique call K-SHREC was developed in this study to map the protein position within the kinetochore by less-than-resolution accuracy.

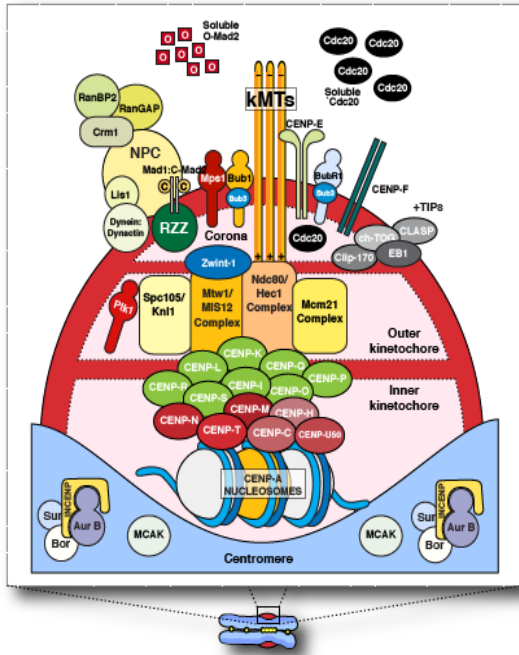


Figure 1.2: Kinetochore proteins

Dissertation layout

Kinetochores were fluorescently labeled to mark to position of chromosome in live cells in order to track the movement of chromosome during metaphase. In Chapter 2 how the kinetochores are detected will be described. In Chapter 3 the methods that accurately measure the coordinates of the kinetochores will be described. In Chapter 4 the tracking algorithm for kinetochore movement will be discussed. In Chapter 5 kinetochore oscillation during metaphase will be characterized. In Chapter 6, I will describe in details about K-SHREC, the method of precisely measuring kinetochore protein positions from the three-dimensional images of fixed HeLa cells at metaphase. In Chapter 6, the discussions and results of the project are also included. In Chapter 7, the design and operation of the SpeckleTracker software will be introduced.

CHAPTER 2

KINETOCHORE DETECTION

Image of kinetochore

The chromosome dynamics study was based on the time-lapse imaging of Ptk1 cells during metaphase (Figure 2.1). Kinetochores appear as bright punctates in the image. The purpose was to establish an effective detection method to specifically distinguish the kinetochore signal from the background. Kinetochore spots have similar size. Although they are generally brighter than the surrounding background, a simple intensity threshold method did not give good detection because of the presence of noise (for example, see Figure 2.2). Sometimes it was possible for noise to reach a similar intensity level as real kinetochore signals. The one distinction is that bright spots resulting from noise have smaller sizes with the appearance of tiny bright dot randomly scattered all over the image.

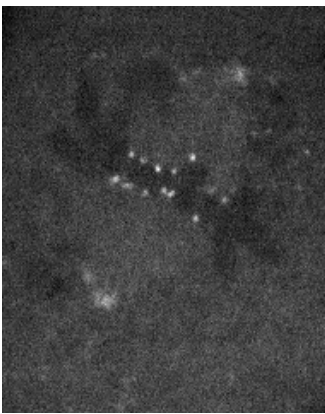


Figure 2.1: Image of kinetochores

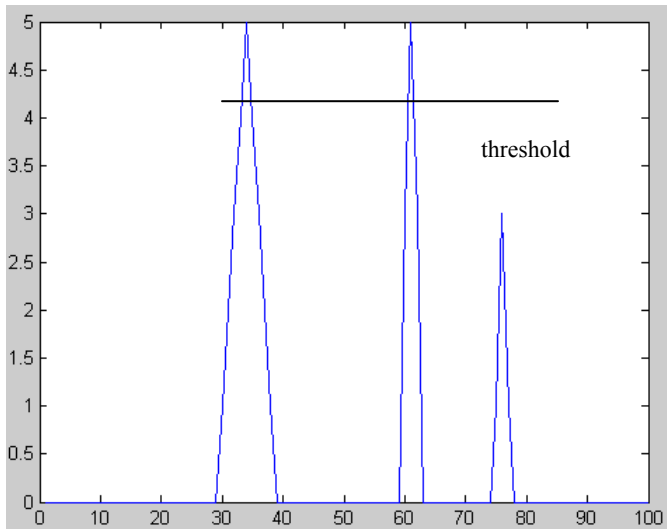


Figure 2.2: Intensity levels of kinetochore and noise

In Figure 2.2, the leftmost peak represents the intensity level of a typical kinetochore. The other two peaks represent noise. It is evident in our image acquisition setting, attributed to the few fluorophores involved in each kinetochore spot, noise sometimes demonstrates intensity levels close to the kinetochore signal. But it is possible to exploit the fact that noise signals have smaller sizes than a kinetochore. In order to efficiently detect kinetochore from a noisy background, an image processing technique called mask (or filter, kernel) was employed.

Methods

A two dimensional mask is a two dimensional array with the organization shown in Table 2.1.

-1	-1	-1
-1	8	-1
-1	-1	-1

Table 2.1: Mask array

When a mask is applied to an image, it moves across the entire image from one pixel to another. Each member in the array corresponds to one pixel in the image. At every position, the operation is performed over the area that the mask covers. The operation is defined by the mask array. The result gives the intensity value of a pixel. It will replace the value of the pixel in the original image that lies in the center of the mask. After the whole process finishes, a new image is generated. The mask above will process an image like this: for each pixel in that image, the new intensity becomes eight times that pixel's intensity value, minus the sum of its surrounding original pixel intensity values. The result is the pixel intensity value of the new image.

The mask method has many applications. It can blur an image to reduce noise. It can also sharpen an image by enhancing edges. The mask used in speckle detection is to blur images.

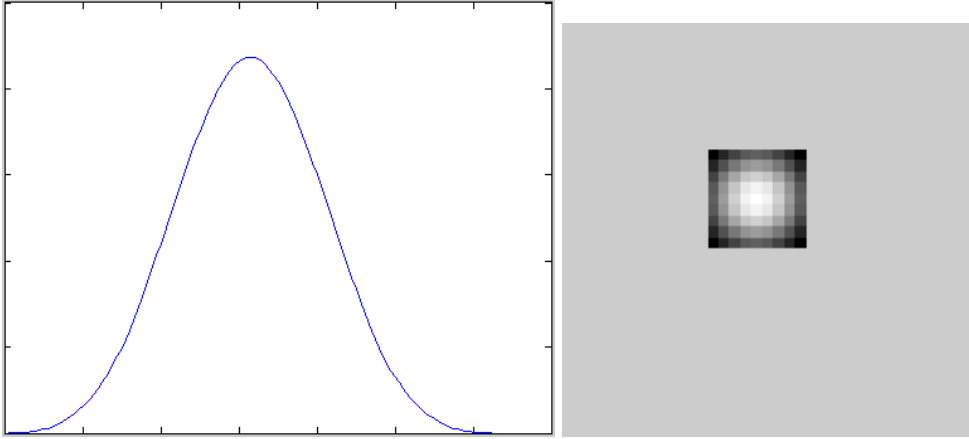


Figure 2.3: Gaussian mask

Figure 2.3 shows the mask used in speckle detection with a profile of a 2-D Gaussian distribution. The mask array (size, 9*9, sigma, 4) is listed in Table 2.2.

0.0067	0.0083	0.0097	0.0107	0.011	0.0107	0.0097	0.0083	0.0067
0.0083	0.0103	0.0121	0.0133	0.0137	0.0133	0.0121	0.0103	0.0083
0.0097	0.0121	0.0141	0.0155	0.016	0.0155	0.0141	0.0121	0.0097
0.0107	0.0133	0.0155	0.017	0.0176	0.017	0.0155	0.0133	0.0107
0.011	0.0137	0.016	0.0176	0.0181	0.0176	0.016	0.0137	0.011
0.0107	0.0133	0.0155	0.017	0.0176	0.017	0.0155	0.0133	0.0107
0.0097	0.0121	0.0141	0.0155	0.016	0.0155	0.0141	0.0121	0.0097
0.0083	0.0103	0.0121	0.0133	0.0137	0.0133	0.0121	0.0103	0.0083
0.0067	0.0083	0.0097	0.0107	0.011	0.0107	0.0097	0.0083	0.0067

Table 2.2: Gaussian mask array

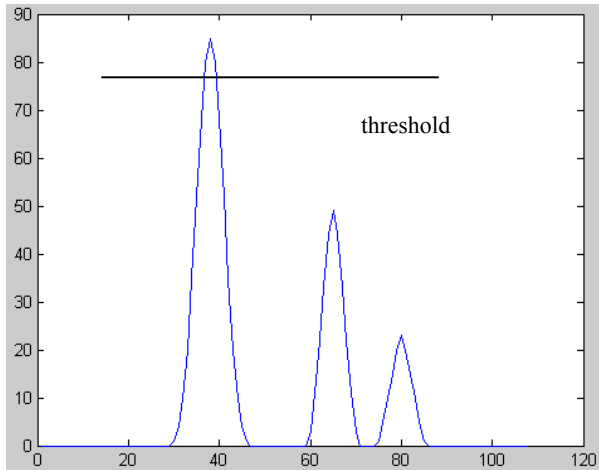


Figure 2.4 Intensity levels of kinetochore and noise after mask operation

The mask is designed to suppress the noise level and therefore enhance the kinetochore signal. After the process the speckle will have distinctively higher peak intensity value than the noise (Figure 2.4, which makes distinguishing between speckle and noise with intensity threshold method more feasible. The peaks in Figure 2.4 are corresponding to the peaks in Figure 2.2. Since the peak intensity of a speckle often lies in the center, the center coordinates can be regarded as the position of that speckle.

A software program was developed to implement such method. The details are given in chapter 7.

CHAPTER 3

ACCURATE MEASUREMENT OF KINETOCHORE POSITION

The accuracy of the kinetochore position obtained from the previous chapter is determined by the resolution limit of optical microscopy, as well as the final pixel size of the camera. However, by implementing Gaussian curve fitting method, it is feasible to further improve the accuracy of kinetochore position information.

Light microscopy

Light microscopy is an essential tool for biological research. Optical lenses are the basic component of a light microscope. The resolution of light microscopy is limited to no less than 210 nm for green light by the objective. A point light source, theoretically is of infinitesimal size, will form diffracted image under the microscope. The function describing such formation is characterized as the objective point spread function (PSF) of that particular microscope setting. PSF is a very critical characteristic of a light microscope. The radius of the PSF determines the resolution of the microscope.

At the focal plane, the intensity distribution of the PSF is given by a second order Bessel function (Figure 3.1). This function usually closely resembles a Gaussian function. And given that a Gaussian function is computationally simpler than a Bessel function, it is common to approximately the infocus PSF as Gaussian function instead.

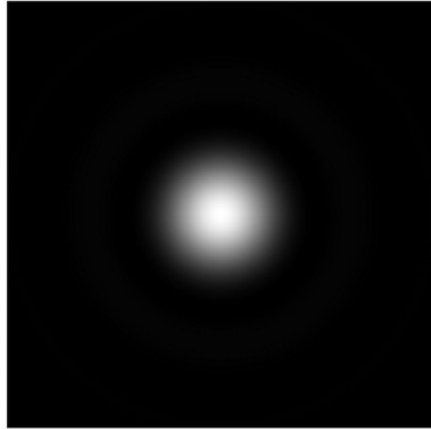


Figure 3.1: Image of PSF

The resolution of a light microscope is determined by the following equation:

$$R = 0.61\lambda / \text{N.A.}$$

λ represents the wavelength of the light. N.A. represents the numerical aperture of the objective of the microscope. For green light ($\lambda = 510 \text{ nm}$), R is about 210 nm. For the spectrum of all the visible light, R generally is greater than 200 nm.

Two-dimensional Gaussian function

PSF can be represented by a two-dimensional Gaussian function as following.

$$f(x, y) = Ae^{-\left(\frac{(x-x_0)^2}{2\sigma_x^2} + \frac{(y-y_0)^2}{2\sigma_y^2}\right)}.$$

PSF is the image of an infinitesimal point light source observed under a microscope. A single fluorophore can be viewed as an infinitesimal light source. A fluorescently labeled kinetochore is assumed to be composed of multiple fluorophores. Therefore, the image of a kinetochore is the convolution product of its fluorophores' position and the objective PSF. Because the size of a kinetochore is much smaller than the size of PSF and the fluorophores are very close to each other, the resulting convoluted image closely resembles the size of a two-dimensional Gaussian function. In other words, the optical signal from a kinetochore can be modeled mathematically as a two-dimensional Gaussian function.

The PSF of a single point source has a circular shape because the point light source is infinitesimal in size. On the other hand, although a kinetochore is very small, it has physical dimensions. Therefore a kinetochore speckle demonstrates a slightly different profile compared to the objective PSF. The speckle may have an elliptical shape due to the fact that one dimension is bigger than the other. In addition, the orientation of the speckle has to be factored in during the computation.

To describe a kinetochore comprehensively, I used a two-dimensional Gaussian function with a rotation transformation to obtain the major and minor axes. As a result, there are seven parameters in total: background level, height of signal (A), centroid positions x_0 , y_0 , sigma σ_x , σ_y and rotation angle (relative to the x-axis in the image).

Least-square curve fitting

The accuracy of the measurement is also limited by the camera pixel size. In this study the pixel size of the camera was ~65 nm. However, a much more accurate measurement can be achieved by applying mathematical methods on the kinetochore signal. One widely used approach is least-square curve fitting of the Gaussian function. The principle of the curve fitting method is as following:

$$\min_x \frac{1}{2} \|F(x, xdata) - ydata\|_2^2 = \frac{1}{2} \sum_{i=1}^m (F(x, xdata_i) - ydata_i)^2$$

For function $F()$ with input data $xdata$ and output data $ydata$, one should find coefficients x that yields smallest difference between the value of function $F()$ and the output data $ydata$. In this case, a Gaussian function $G()$ that is to be fitted, $xdata$ represents the coordinates of a kinetochore image, and $ydata$ represents the image intensity levels, while x represents the collection of the seven parameters described in the previous paragraph.

A MATLAB (The Mathworks, Natick, MA) function “lsqcurvefit” was employed to perform two-dimensional Gaussian curve fitting. The format is as following:

`[x,resnorm] = lsqcurvefit(fun,x0,xdata,ydata,lb,ub)`

where 'fun' represents the two-dimensional Gaussian function; 'x0' represents the initial estimated values of the seven parameters; 'xdata' represents the coordinates of the two-dimensional image in the region of interest (ROI). 'ydata' represents the intensity reading of single pixels.

'lb' in the formula represents the lower bounds of the possible 7 parameters. Regarding coordinates, the lower bounds are the minimal values of the coordinates in the ROI.

Regarding sigma values, the lower bounds are set as one eighth of the estimated sigma value input by the user. For rotation angles, the lower bounds are set as -360 degree. The lower bound of the bottom of the Gaussian is half of the minimal value among the image pixels in the ROI. The lower bound of Gaussian height is set to 1. 'ub' in the formula represents the upper boundaries. Regarding the coordinate parameter, the upper bounds are the maximum values of the area of interest coordinates. Regarding sigma values, the upper bounds are set as four times higher than the estimated sigma value by user's input. Regarding rotation angles, the upper bounds are set as +360 degree. The upper bound of the bottom of the Gaussian function is set twice higher than the minimal value among the pixels in the ROI. The upper bound of Gaussian height is set as 1.5 times higher than the peak value within the ROI.

The setting choices for lower bound and upper bound values were made in such way to provide enough room for the fitting process to find the optimized answer, but not too large to avoid an unreasonable amount of computation time when executing the program.

The centroid from the fitting results is then viewed as the position of the kinetochore. A software program in MATLAB was developed to perform the continuous tracking of the dynamic position of the centroid (Chapter 7). The details of the algorithm are disclosed in Chapter 4.

Three-dimensional Gaussian fitting

The method described above is for two-dimensional image data. To accurately locate a kinetochore in three-dimensional images, similar approaches were implemented for three-dimensional image stacks. Three-dimensional Gaussian functions replaced the two-dimensional Gaussian function. 3 more parameters were needed: sigma value of z axis, centroid coordinate of z axis and one more rotation angle. Other parameters remained the same. The three-dimensional Gaussian fitting method was essential in the study of K-SHREC, which will be discussed in Chapter 6.

CHAPTER 4

KINETOCHORE TRACKING

Introduction

The best way to study the dynamics of cellular activity is to utilize live cell imaging techniques. Studies of the dynamics of chromosome movement are essential in the research of mitosis. Kinetochores are often fluorescently labeled to reveal the movements of chromosomes. Effective tracking of the kinetochore movement is the first step in the study.

The subject of object tracking covers a large area, from the tracking of simple objects, like stars, to the tracking of complicated movements, like the running of athletes.

Kinetochore tracking is in the area of point tracking, a subcategory of object tracking, where objects can be simply represented by points. The detection method listed in the previous chapter identifies kinetochore as points and yields the coordinates. The purpose of the tracking is to connect the points from different frames and find the correspondence for the same point in different frames.

Figure 4.1 shows the basic idea of tracking. From frame 1 to frame 3, 9 kinetochores (objects) were detected. They were represented by 9 points, from point 1 to point 9. The purpose of tracking is to figure out which points in different frames are the same one. In

other words, for example, which point (4, 5 or 6) in the second frame is related to point 1?
Which point (7,8 or 9) in the third frame is related to point 4?

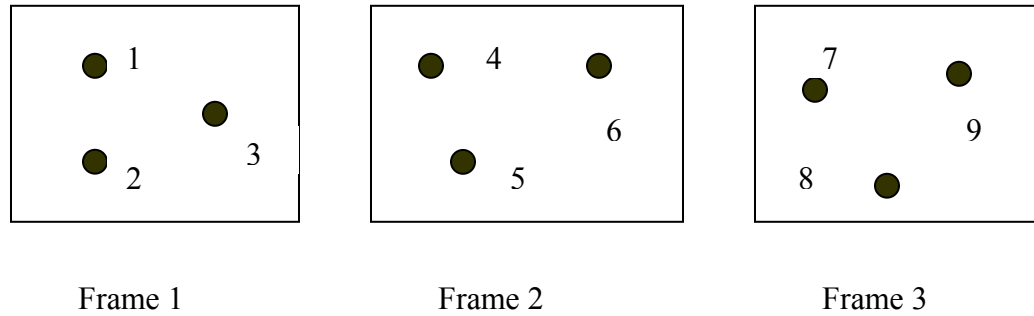


Figure 4.1: Points from different frames

A good tracking method or algorithm will give you the results like this, 1, 4 and 7 are the same one; 3, 6 and 9 are the same one, as well as 2, 5 and 8. Based on the tracking results, the same point in a different frame will have the same label (Figure 4.2).

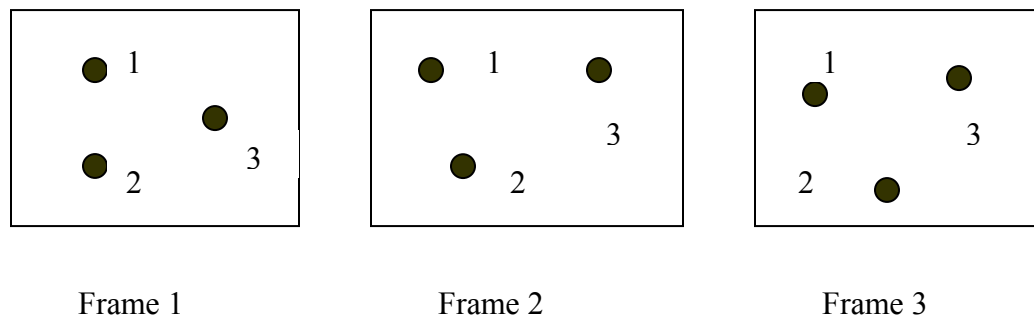


Figure 4.2: Point tracking

Methods

Some existing tracking methods are applicable for kinetochore tracking.

1). Nearest neighbor method

The nearest neighbor method is simple; just find the closest point in the next frame and consider it as the same one. It is simple to understand and easy to implement. In Figure 4.3, the closest one to point 3 of frame 1 in frame 2 is point 6. We can also quickly find the correspondence between 1 and 4, 2 and 5 in the same way. Correspondence between frame 2 and 3 can also be easily established without any trouble.

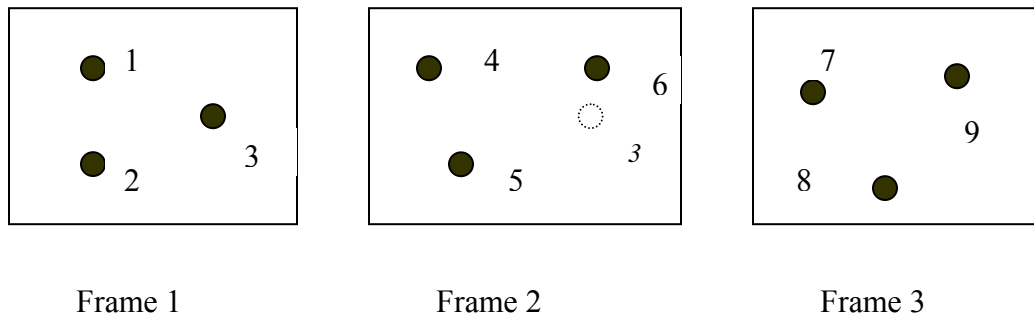


Figure 4.3: Nearest neighbor method

However, the nearest neighbor method doesn't always give the right results. In Figure 4.4, Point 3 in frame 1 has its nearest neighbor to point 1 in frame 2. This will generate false correspondence. Nearest neighbor method is limited to the situation where points are generally close to each other and don't have big movements between two adjacent frames. In order to track points with various movements, different methods are adapted.

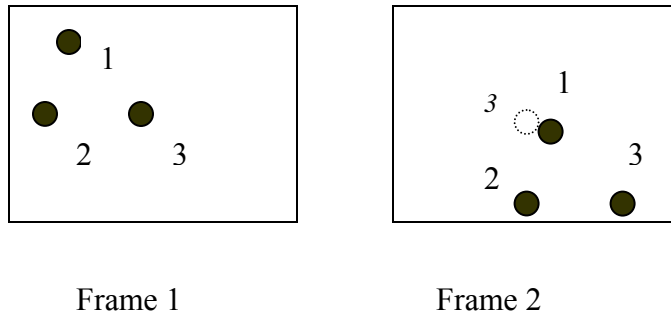


Figure 4.4: Limit of nearest neighbor method

2). Minimum square distance

When there are not too many points in one frame, reviewing each and every possible correspondence is a task that can be realized. Table 4.1 below lists all the six possibilities of correspondences for Figure 4.5. Only one of them is the right answer. In this method, sum of the square distance for all the correspondences are calculated. For possibility 1 in the table, the calculation is the following:

$$S1 = (\text{distance between 1 \& 4})^2 + (\text{distance between 2 \& 5})^2 + (\text{distance between 3 \& 6})^2$$

For the other five possibilities, calculations for S2, S3, S4, S5, and S6 are done in the same way. The S with the minimum value is picked as the right answer. The square distance can apply to the two adjacent frames only or all the frames all together. For square distance over all the frames, all the possible correspondences need to be evaluated.

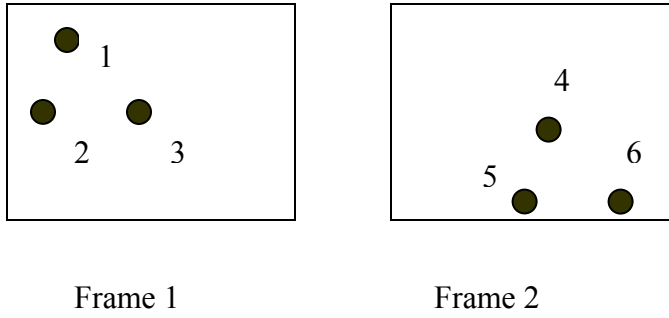


Figure 4.5: Minimum square distance method

1	1&4, 2&5, 3&6
2	1&4, 2&6, 3&5
3	1&5, 2&4, 3&6
4	1&5, 2&6, 3&4
5	1&6, 2&4, 3&5
6	1&6, 2&5, 3&4

Table 4.1: List of all possible matches

3). Weighted minimal distance

It is similar to method 2). A weight (w) is assigned to each squared distance (Thomann, et al., 2002). Each weight is different. The minimal sum of the weighted squared distances is selected from all possible correspondences.

$$S1 = w1*(\text{distance between 1 \& 4})^2 + w2*(\text{distance between 2 \& 5})^2 + w3*(\text{distance between 3 \& 6})^2$$

New methods were studied based on the movement of kinetochores.

1). Kinetochores move in similar motion. Because the movements are similar, their squared distance should be close to one another. Therefore, the standard deviation of the squared distance should be small. Minimal standard deviation of the squared distance was developed.

2). Kinetochores move only in two directions: towards and away from the pole. The two directions of oscillation are almost opposite to each other. Figure 4.6A illustrates the directions of the movement between two frames.

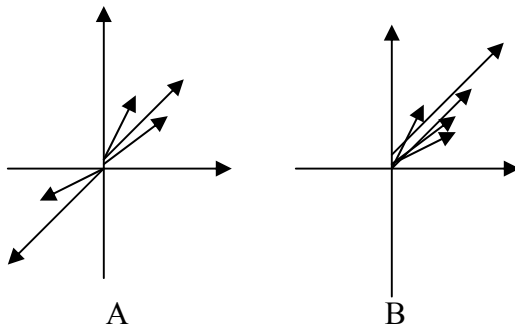


Figure 4.6: Kinetochores movement vectors

In Figure 4.6B, by switching the opposing vectors 180 degree, all the vectors point to one direction. Based on this result, an algorithm was introduced: first find all the possible matches within the maximum movement radius. For each match turn movement vectors in quadrant I, II (or III, IV) by 180 degree into quadrant III, IV (or I, II). Then find the match with minimum standard deviation of the vector angles. Those vectors only

represent fast poleward movement. Not every kinetochore moves that way. The vectors from slow or stationary kinetochores have different angles. To minimize the influence of those non-poleward movements, weighted least squared error was used. V_i represents the angle of the i th movement vector in one possible match between two consecutive frames. V_m is the mean angle of all the movement vector angles of that match. L_i is the norm of the i th vector. Weighted least squared error for all the candidates are calculated. The one with minimal error is selected.

$$\min \sum L_i (V_i - V_m)^2$$

Tracking can constantly run into trouble when the situation becomes complicated.

1) When there are large number of points for each frame.

If all the possible correspondences can be obtained and valued, the best one that meets the criteria by the tracking method will be considered the correct answer. However in reality, the total number of possibilities can be really huge, and reviewing all the candidates becomes an impossible task. For example, tracking m points with n frames, the total number of candidates are $(m!)^n$. Just for 10 points at 10 frames, the number can be 3.96×10^{65} .

2) When point(s) become missing in the next frame(s).

Sometime, point(s) can suddenly disappear. In Figure 4.7, point 1 disappears in frame 2. This scenario is fairly common for microscopy imaging since objects frequently move in and out focus.

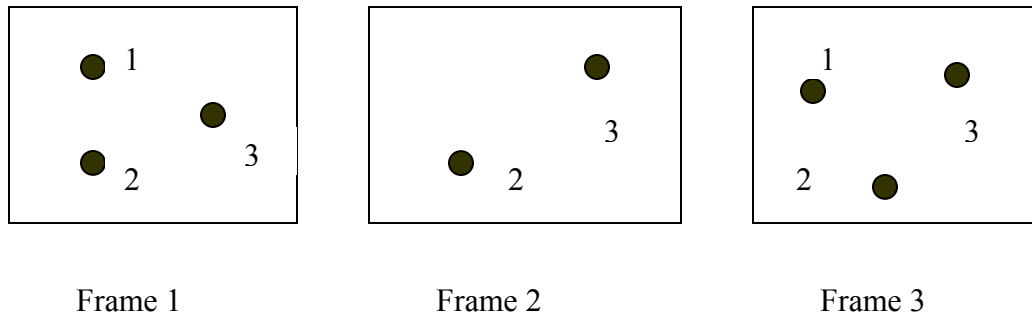


Figure 4.7: Tracking problem: point missing

During tracking, one point in frame 1 and 3 will not have its corresponding point in frame 2. If the point 1 never appears again after frame 1, no tracking is necessary for it. If point 1 reappears, then correspondence needs to be established.

3) When new point(s) emerge in the next frame.

Sometime point(s) that don't exist at the previous frame can appear in the next frame. In Figure 4.8, there is no point 3 in frame 1 but it shows up in frame 2.

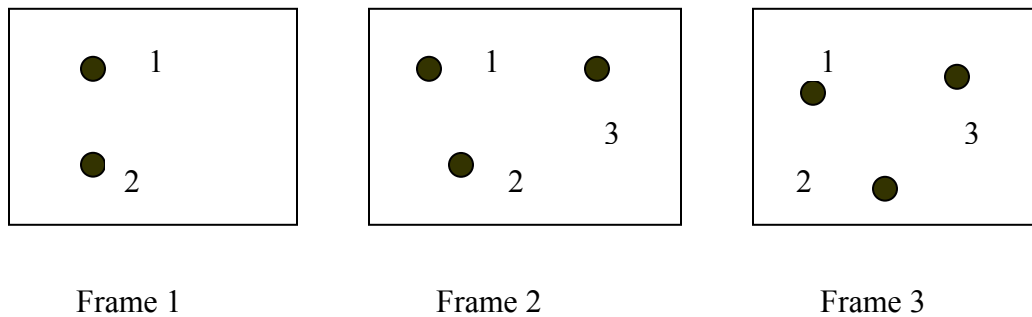


Figure 4.8: Tracking problem: point emerging

One point in frame 2 will not have its corresponding point in frame 1. This situation is similar to the reappearing of point 1 in frame 3 from Figure 4.6.

When there are point(s) coming in or out of a frame, the tracking method needs to have the capability to tell which one is disappearing, which one is a new comer and which one is just reappearing.

4) When two or more points overlap with each other.

Two or more points may also overlap. In Figure 4.9, point 2 and 3 run into each other in frame 2.

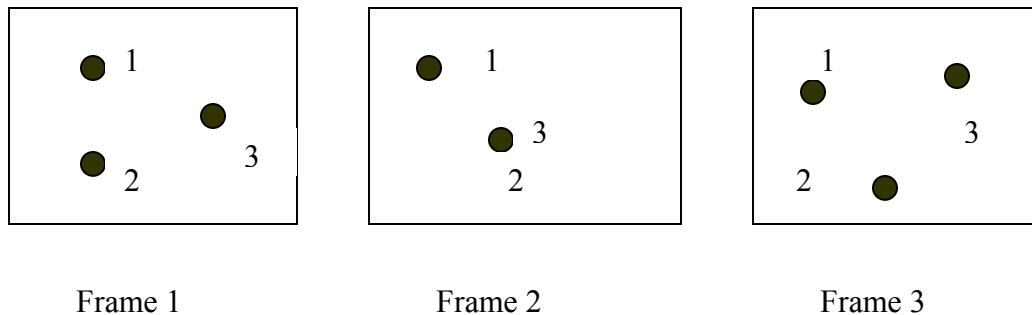


Figure 4.9: Tracking problem: points overlapping

In such case, one point in frame 2 will have two corresponding points in frame 1. To make things worse, such case just looks the same as one point disappearing in frame 2. Sometime it is really hard to tell if there is one point disappearing or two points merging.

Results

Three methods were tested in this project, weighted least-squared error of movement vector angle, minimal sum of squared distance and minimal deviation of squared distance. Totally 25 frames from three different kinetochore image sequences were tested. Tables 4.2, 3 and 4 show the results from three movies based on the three methods. Tracking was performed between two consecutive frames.

frame # (# of points)	# points leaving from last frame	# points entering this frame	Results (# of wrong matching points)		
			min dev(dis ²)	weighted angle	min Σ dis ²
1 (16)					
2 (15)	1	0	0	0	0
3 (15)	0	0	0	0	0
4 (15)	1	1	4	6	3
5 (16)	0	1	0	0	0
6 (16)	0	0	0	8	0
7 (15)	1	0	0	0	0
8 (15)	0	0	0	0	0
9 (16)	0	1	0	0	0
10 (16)	0	0	0	0	0
155		Total:	4	14	3

Table 4.2: Tracking results of image sequence 1

frame # (# of points)	# points leaving from last frame	# points entering this frame	Results (# of wrong matching points)		
			min dev(dis ²)	weighted angle	min Σ dis ²
1 (12)					
2 (13)	0	1	1	0	1
3 (13)	0	0	0	3	0
4 (14)	0	1	2	3	2
5 (13)	1	0	0	2	0
6 (12)	1	0	0	0	0
7 (14)	0	2	0	2	0
8 (13)	1	0	4	2	4
9 (14)	0	1	2	2	2
10 (14)	0	0	0	0	0
132		Total:	9	14	9

Table 4.3: Tracking results of image sequence 2

frame # (# of points)	# points leaving from last frame	# points entering this frame	Results (# of wrong matching points)		
			min dev(dis ²)	weighted angle	min Σ dis ²
1 (12)					
2 (12)	0	0	0	2	0
3 (15)	0	3	0	0	0
4 (16)	0	1	0	4	0
5 (16)	0	0	0	2	0
71		Total:	0	8	0

Table 4.4: Tracking results of image sequence 3

As shown in Tables 4.2, 3 and 4, minimal sum of squared distance and minimal standard deviation methods gave better results than weighted least-squared error of angle. And those two methods gave almost the exact same performance. Only in the tracking between frame 3 and 4 in image sequence 1 (Table 4.2), was minimal sum of squared distance slighter better. This is also the case for points entering and leaving at the same time. For the rest of the sequence, the two methods gave exactly the same performance.

Results also show that the two squared distance based methods work well on frames when points leaving and entering don't happen at the same time. In Figure 4.10, point 13 and 14 in right image are just entering that frame. They can be successfully identified.

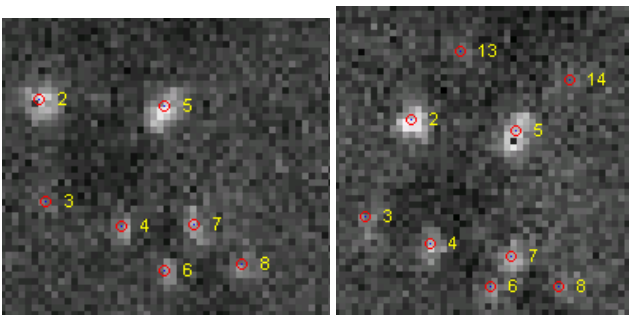


Figure 4.10: Good tracking results (frame 6 (left) and 7 (right) in sequence 2)

In Table 4.3, from frame 3 to frame 4, points are entering and leaving at the same time.

All methods gave very poor results.

Table 4.4 shows that tracking for image sequence 2 had more errors than the tracking of image sequence 1 and 3. After examining the errors and comparing them to good results, one major difference was found. Points moved farther in those mis-tracked frames. There were larger displacements.

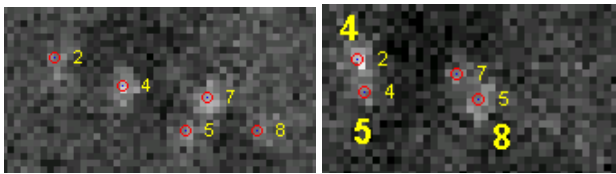


Figure 4.11: Bad tracking results I (frame 7 (*left*) and 8 (*right*) in sequence 2)

Another factor that has a negative effect on that result was that there was a point leaving (Figure 4.11). Point 2 in left image is leaving but the tracking methods failed to detect that. The right answer is shown in big font in the right image.

Most errors made by weighted least squared angle error method were mismatching between two points in a pair. In Figure 4.12, point 4,6; 11, 12; 10,16 on top frame should be 6,4; 12,11; 16, 10 on the bottom respectively.

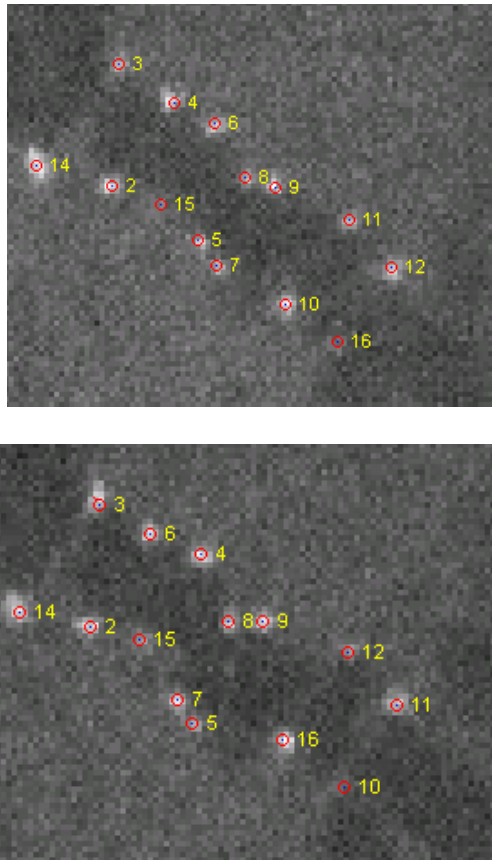


Figure 4.12: Bad tracking results II (frame 5 (*top*) and 6 (*bottom*) in sequence 1)

Maximum movement radius is an important parameter that needs to be defined before tracking. It should be large enough to cover the area where fastest point doesn't move out of such area, but also not be too large to make the candidate list too long. In this study, it was set to 15 pixels to all the three sequences.

Discussions

Because kinetochores coming in and out of focus and overlapping are quite common, dealing with such issues makes tracking extremely difficult. It is also impossible to have a 100% accurate tracking method. Further correction is an important aspect in the whole

tracking process. Two factors together make nearest neighbor method a good choice from the software design perspective. It is simple to use. Tracking errors can also be easily corrected. Details about how to track kinetochores and how to edit tracking results are in the software development chapter (Chapter 7).

CHAPTER 5

CHROMOSOME DYNAMICS IN METAPHASE

Abstract

Kinetochores of mitotic cells are known to oscillate during prometaphase and metaphase. By analyzing time-lapse movies of late prometaphase or metaphase cells undergoing mitosis recorded by fluorescent confocal microscopy techniques, I was able to acquire more insights about the oscillation mechanism. For sister kinetochore pairs, their oscillating frequencies and periods were analyzed by a Fourier transform approach. This analysis showed that the oscillating frequency between sister kinetochores is about 2 times higher than the oscillating frequency between kinetochores and their poles. As a result, kinetochore oscillations cannot be modeled by simple sine waves, in which case the two oscillating frequencies described above would be equivalent. High resolution tracking also revealed an asymmetric pattern between a kinetochore's poleward (P) motion and away-from-the-pole (AP) motion. On average, kinetochores move faster in P motion than in AP motion; the period of P motion is shorter than the period of AP motion, neither being with constant moving rate. In addition, P motion and AP motion have a different position versus time relationship, which indicates they are produced by different mechanisms. Sister kinetochores also oscillate with different phases relative to each other. The leading kinetochore usually switches first from P to AP motion while the trailing kinetochore switches second from AP to P motion. This asymmetry and relative phase

difference between sister oscillation is why centromere stretch oscillates at twice the frequency of individual sister kinetochores.

Methods

Time lapse imaging of Ptk cells in metaphase was used in this study. The kinetochore marker was Alexa488-labeled antibody to CenpF, a peripheral kinetochore protein (Figure 5.1). Time-lapse images were acquired as described by Cimini et al., 2004 and Cameron et al. 2006, using a spinning disk confocal microscope.

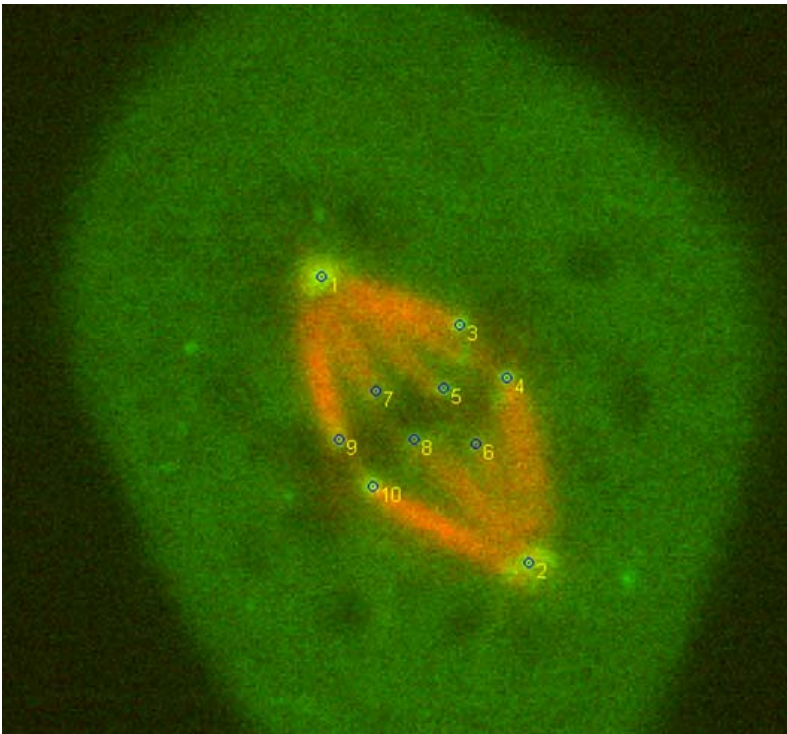


Figure 5.1: Measured and labeled kinetochores

Kinetochore pairs were detected (Chapter 2 and 3) and then tracked (Chapter 4) with Speckletracker software (Chapter 7). Spindle poles were identified in the similar fashion.

For convenience, poles were always labeled with number 1 and 2. Kinetochores were labeled in 3 and 4, 5 and 6, 7 and 8, etc.

Results

The distance between kinetochore and pole (k1p1 and k2p2) was calculated and plotted along with the distance between the sister kinetochores pair, or K-K distance (Figure 5.2).

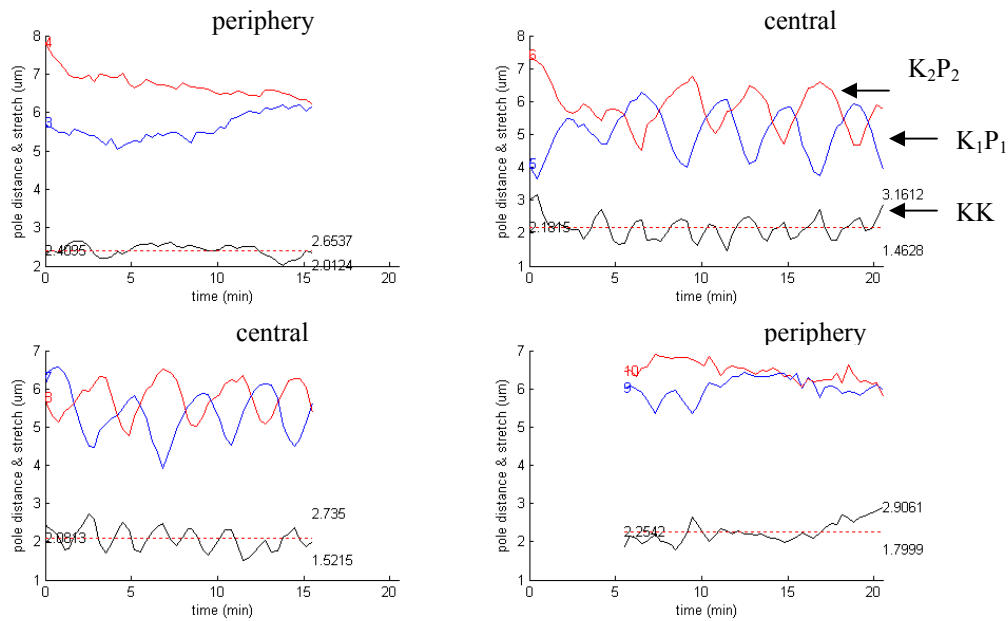


Figure 5.2: Distance between kinetochore and pole (red and blue line) and distance between sister kinetochores

Kinetochore Pair and K-K Oscillations

The oscillation pattern is very clear for some kinetochore pairs (Figure 5.2). Not only do the kinetochores oscillate relative to the spindle, but also K-K distance demonstrates similar regular oscillation pattern. Note, for unknown reasons (Cimini et al., 2004, Cameron et al., 2006) chromosomes of the spindle periphery (e.g. 3,4; 9, 10 in Figure 5.1)

exhibit little and irregular oscillations compared to the majority in the middle of the spindle (e.g. 5, 6; and 7, 8 in Figure 5.1). Our focus is on the oscillating chromosomes.

Power Spectrum Analysis

To look further into such phenomenon, oscillation frequency was calculated (Figure 5.3). The oscillation frequency of K-P distance and the oscillation frequency of K-K distance were obtained by Fourier Transform. The results show that K-P oscillates at around 4 minutes per cycle and K-K distance oscillates at 2 minutes per cycle. The K-K oscillation period is exactly the half of the K-P oscillation, or the frequency is doubled.

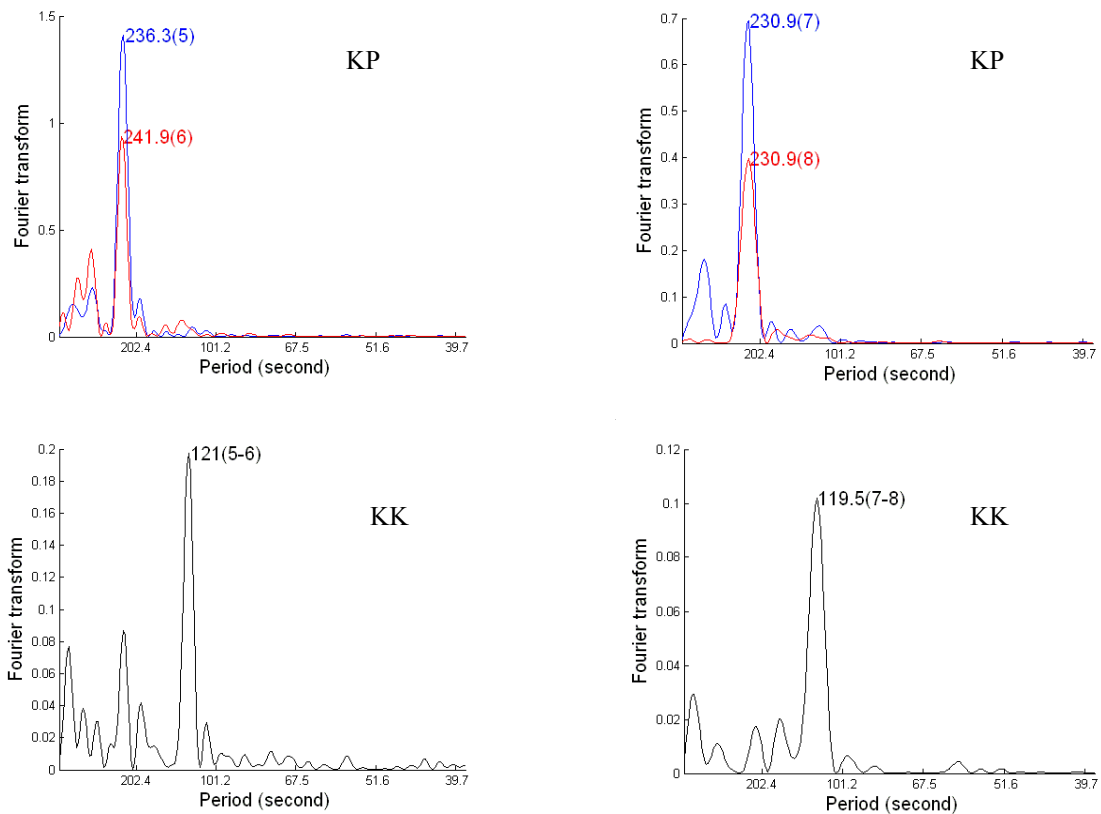


Figure 5.3: Oscillation frequencies

Analysis of different kinetic models

First, I considered pure sine wave oscillations. When K-P oscillates at sine wave motion, the K-K distance between a sister kinetochore pair also oscillates with sine wave motion (Figure 5.4A). However, the frequencies of both oscillations are the same. If the K-P oscillation pattern is a triangle wave with the same slopes of up and down, the K-K distance oscillates with a rectangular, the frequency remains the same as K-P oscillation (Figure 5.4B). In the third model, oscillation is triangle wave, but the up and down slopes are different so that the phase durations between the up and down movements are different (Figure 5.4C). This produces K-K oscillations with double the frequency of K-P oscillations. In first and second model, no matter how much shift between phases of sister kinetochore oscillations occur, the K-K frequency remains the same.

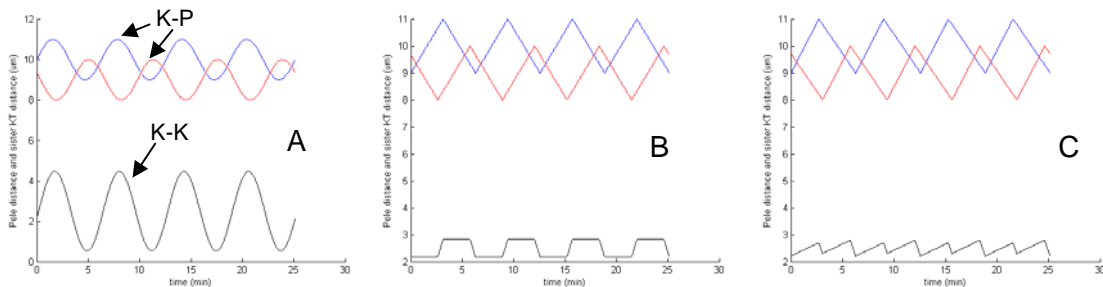


Figure 5.4: Oscillation models

Asymmetry between P and AP movements is the main cause. In (A) sister kinetochores have sine wave oscillation patterns with identical frequency but different phase. The sister kinetochore distance has the same oscillation frequency. (B) is similar to (A), but the sister kinetochore have triangle wave oscillation. Both (A) and (B) have symmetric

kinetochore P and AP movements. (C) has asymmetric P and AP pattern with different phase between the sisters. In (C), the sister kinetochore distance frequency is doubled.

Velocity and Duration Measurements of Kinetochore P and AP phases

During one oscillation cycle, the movement of a kinetochore can be divided into two parts. One is the poleward motion (P motion). The other is away-from-the-pole motion (AP motion). The average velocities and periods of the two motions are listed in Table 5.1.

Measurement show that the velocity and period of P and AP movements are different (Table 5.1), indicating P movement and AP movement are asymmetric. Since on average a kinetochore comes back to its start position when it finishes one full oscillation cycle, including one P and one AP movement, the average distance travelled or the average oscillation periods for P and AP movement are the same. When P movement shows 20% increase in velocity relative to AP movement, its period will become 20% shorter (Table 5.1).

	P motion	AP motion
Velocity ($\mu\text{m}/\text{min}$)	1.09 (0.36)	0.88 (0.26)
Period (min)	1.59 (0.51)	1.85 (0.69)

Table 5.1: P and AP velocities and periods

Which sister kinetochore switches first?

The exact mechanism of kinetochore oscillation during metaphase is still unknown (Maiato et al., 2004). What causes kinetochore switching from P to AP motion and then back to P motion is a major piece of the puzzle. There are three critical time points during kinetochore oscillation: switching point from P to AP motion, switching point from AP to P motion and the time when maximum K-K distance occurs. The maximum K-K distance represents the maximum tension produced by the stretch of the centromere inbetween sister kinetochores. Understanding the sequence of the three events may give us some insights about the oscillation mechanism.

These three time points can be extracted from the oscillation plots (Figure 5.2). Turning points (peaks and valleys) on the K-P and K-K curves were recorded. Peaks of the K-K curves reveal maximum tension. Peaks of the K-P curves are the switching points of AP to P motion. Valleys of the K-P curves are the switching points of P to AP motion. When a kinetochore is in P motion, it is also called leading kinetochore. When a kinetochore is in AP motion, it is also called a trailing kinetochore. K-K distance also represents centromere stretch. The centromere rest length is about 1 μm in Ptk1 cells.

- 1). leading KT switching and trailing KT switching

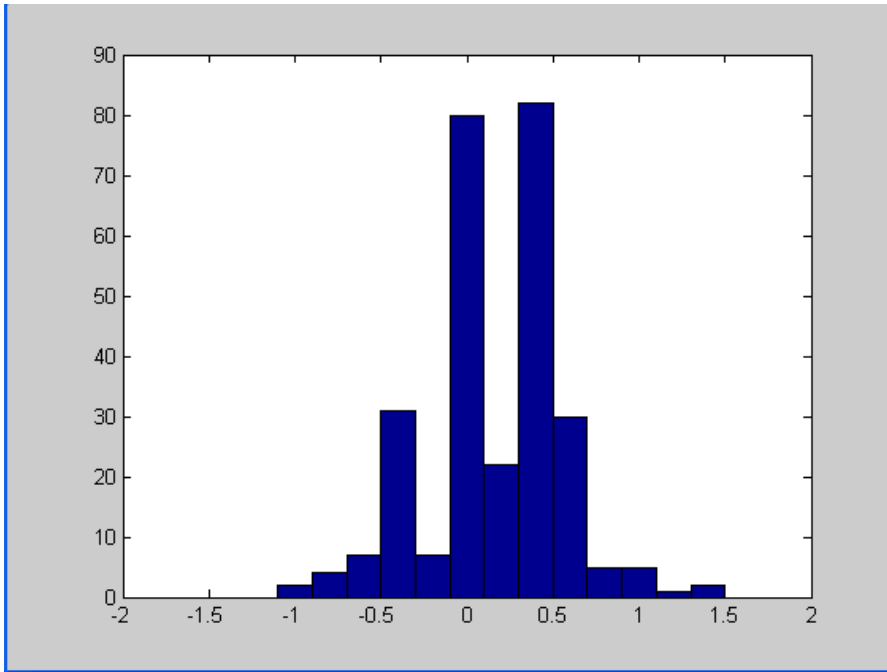


Figure 5.5: Histogram of time difference between leading KT switching and trailing KT switching. X axis shows the time difference (minutes) of the switching between two kinetochores in a sister pair. + means the leading kinetochore switches first, - means trailing first switches.

Figure 5.5 shows that:

- 1). 28.06 %: leading and trailing KTs switch at the same time.
- 2). 53.24 %: leading KT switches first (average 0.43 min).
- 3). 18.71%: trailing KT switches first (average 0.41 min).

On average, leading KT switches direction 0.15 minutes ahead of trailing KT switches direction.

- 2). leading KT switching and max K-K distance

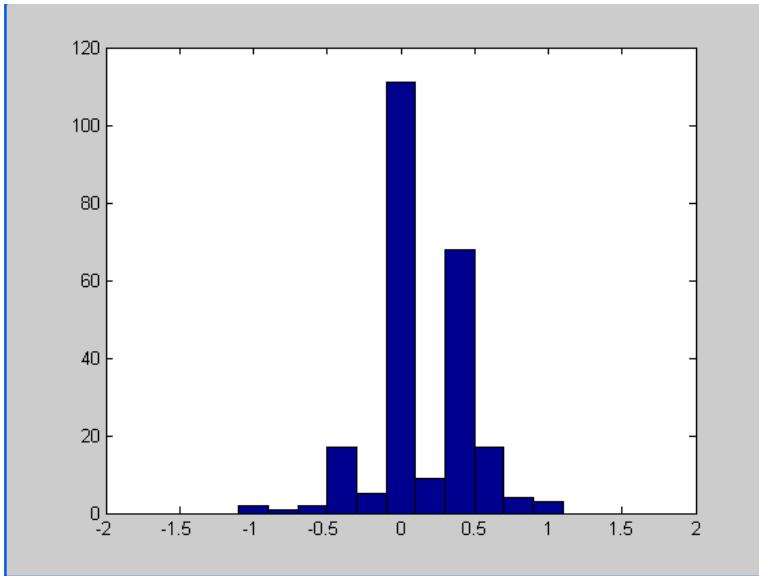


Figure 5.6: Histogram of time difference between leading KT switching and max K-K distance. + means K-K distance happens first, - means leading kinetochore switches first. The X scale is in minute.

Figure 5.6 shows that:

- 1). 45.61%: leading KT switching and max stretch happen at the same time.
- 2). 43.10%: max stretch happens before leading KT switching (average 0.41 min).
- 3). 11.30%: max stretch happens after leading KT switching. (average 0.40 min).

On average, maximum tension between sister kinetochore (maximum K-K distance) happens 0.13 minutes ahead of leading KT switching.

- 3). trailing KT switching and max K-K distance

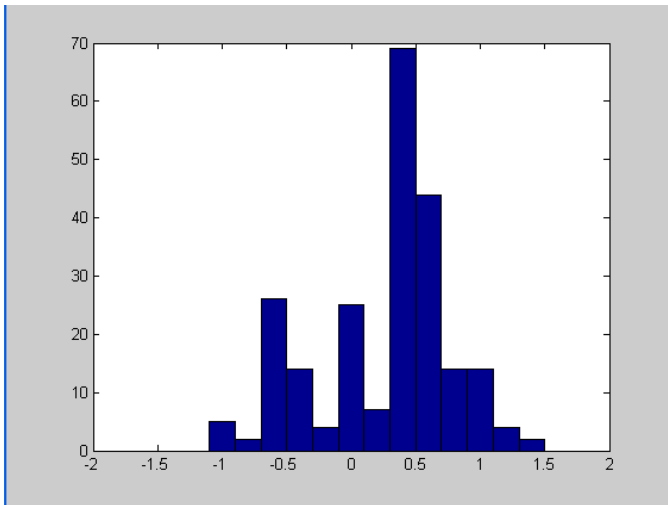


Figure 5.7: Histogram of time difference between trailing KT switching and max K-K distance. + means K-K distance happens first, - means trailing kinetochore switches first. The X scale is in minute.

Figure 5.7 shows that:

- 1). 10.43%: trailing KT switching and max stretch happen at the same time.
- 2). 66.96%: max stretch happens before trailing KT switching.
- 3). 22.61%: max stretch happens after trailing KT switching.

On average, maximum tension happens 0.25 minutes ahead of trailing KT switching.

The results above clearly show that maximum stretch happens first, then leading kinetochore switches and trailing kinetochore switches last. This may imply that centromere stretch may be the trigger to cause kinetochore to switch from P to AP motion.

The average time difference of first and second events, max stretch and leading KT switching respectively, is 0.13 minutes. The average time difference of second and third events, leading KT switching and trailing KT switching respectively, is 0.15 minutes.

Then the average time difference of first and third events should be $0.13 + 0.15 = 0.28$ minutes. The result was 0.25 minutes. They are very close.

The switching time difference between the leading kinetochore and the trailing kinetochore also represents the phase difference between P movement and AP movement.

Characterization of P and AP motions

For each and every P and AP motion, the oscillation period is different from one another. This is also true for the oscillation amplitude. Normalization was used to combine all the data together. All the individual P and AP movement was normalized to have a period of 1 and amplitude of 1.

All the P motion data were then plotted together (Figure 5.8). Polynomial curve fitting was used to find P motion kinetic curve. AP motion kinetic curve was derived by the same method (Figure 5.9). The difference between the two curves is shown in Figure 5.10. Because the exact functions of P and AP kinetic curves are unknown and any function can be expressed by Taylor series, a polynomial function, polynomial fitting was selected as an unbiased approach. 5-degree polynomial functions were used in all the fitting. When the degree was higher than five, the smoothness of the curve was lost. When the degree was lower than 5, the function was too simple to fully reveal the dynamics of P and AP movements.

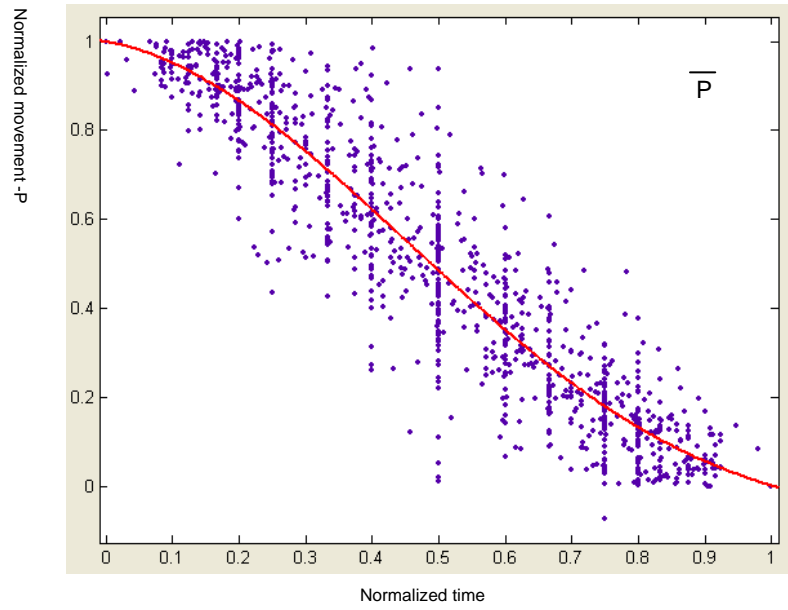


Figure 5.8: P kinetic curve

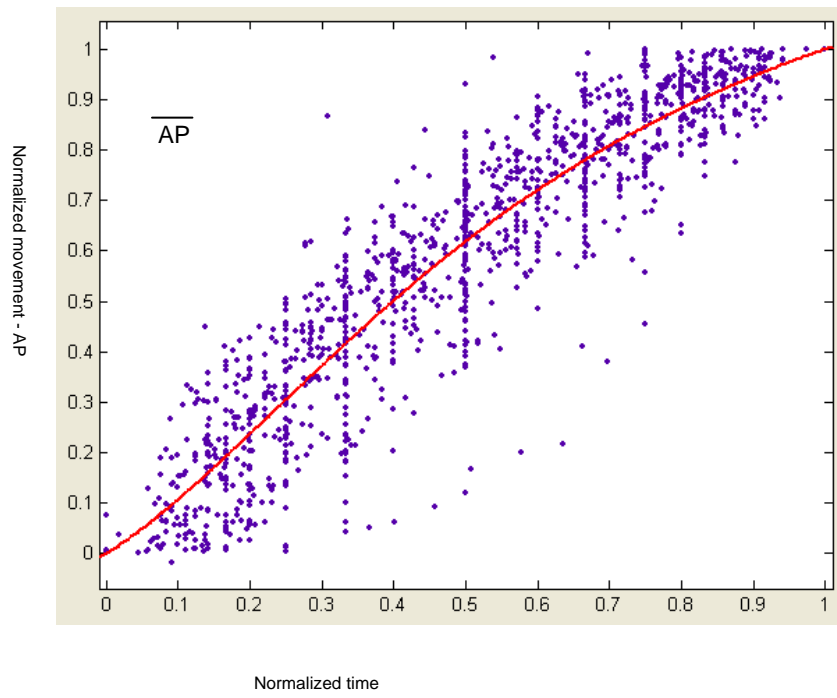


Figure 5.9: AP kinetic curve

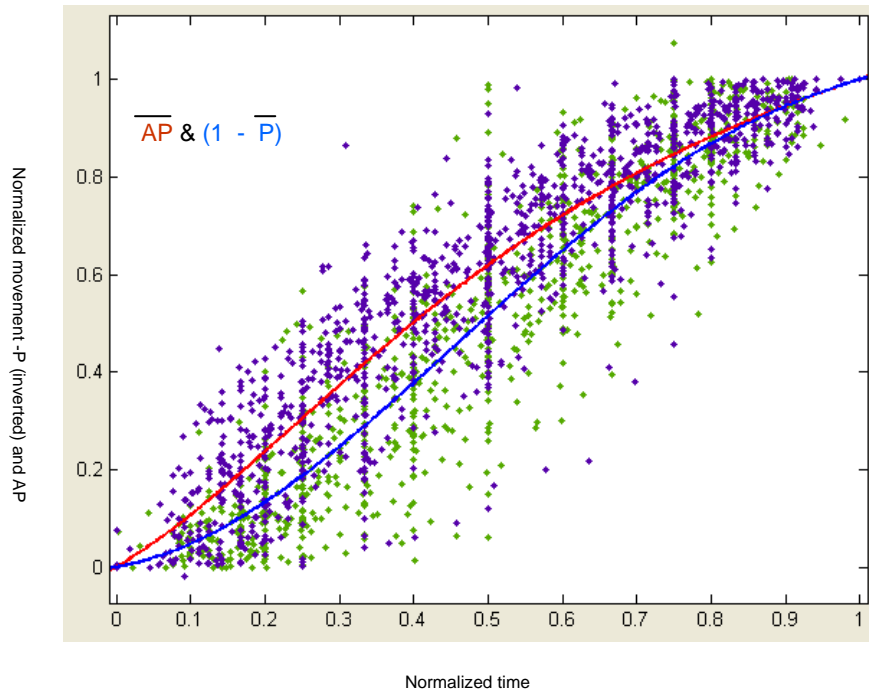


Figure 5.10: P and AP kinetic curves

We can also speculate the velocity of P and AP motion at every point of the movement (Figure 5.11). The velocity curve was obtained from the derivative of the characteristic curve. Limitation of curve fitting and normalization can only make speculative claim over the velocity. But the difference between the kinetic pattern of P and AP motion is significant.

Kinetochose oscillations in monopole spindles

The same approach for analysis of kinetochose oscillations in monopole spindles yielded similar results for P and AP motion (Figure 5.12). The P movement kinetic curve in monopole spindles is very close to the P movement kinetic curve in bi-pole spindles. The AP movement kinetic curve for monopoles also looks very similar to the AP movement

kinetic curve for bi-pole spindles. However, in monopole spindles, the frequency of kinetochore oscillation is faster than that in bi-pole spindle.

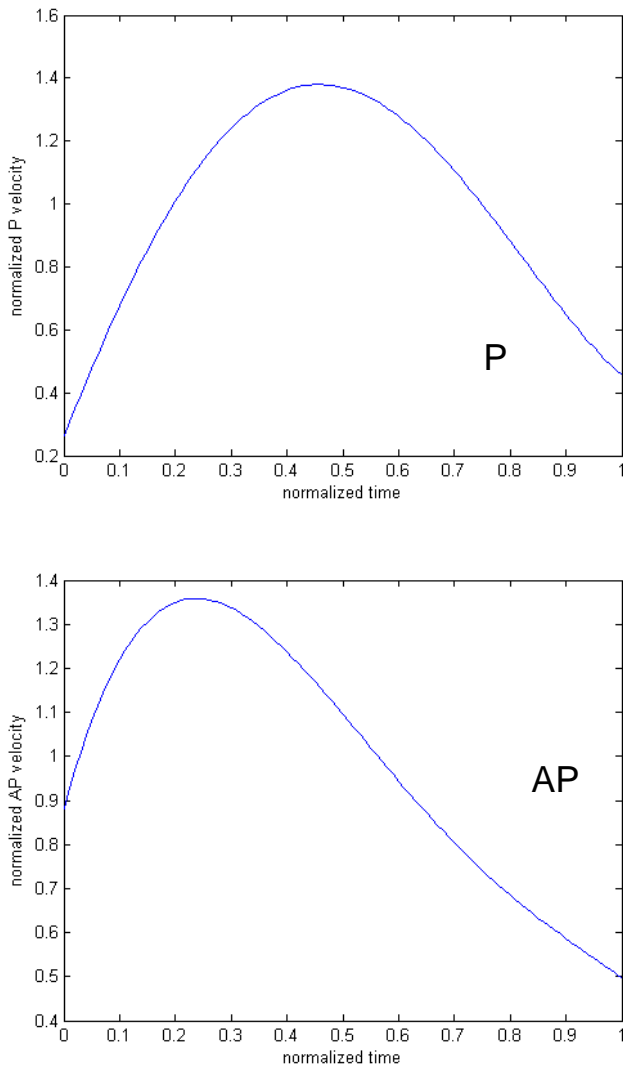


Figure 5.11: P and AP velocity curves

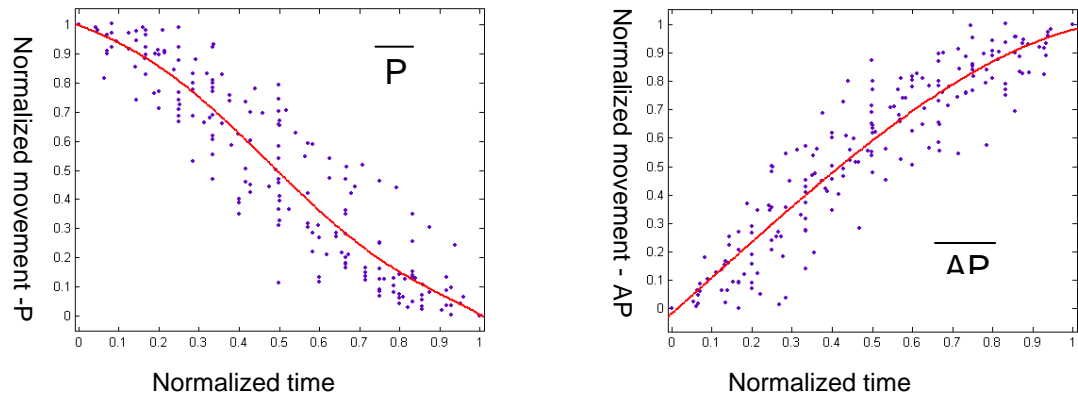


Figure 5.12: P and AP movements of monopole spindle

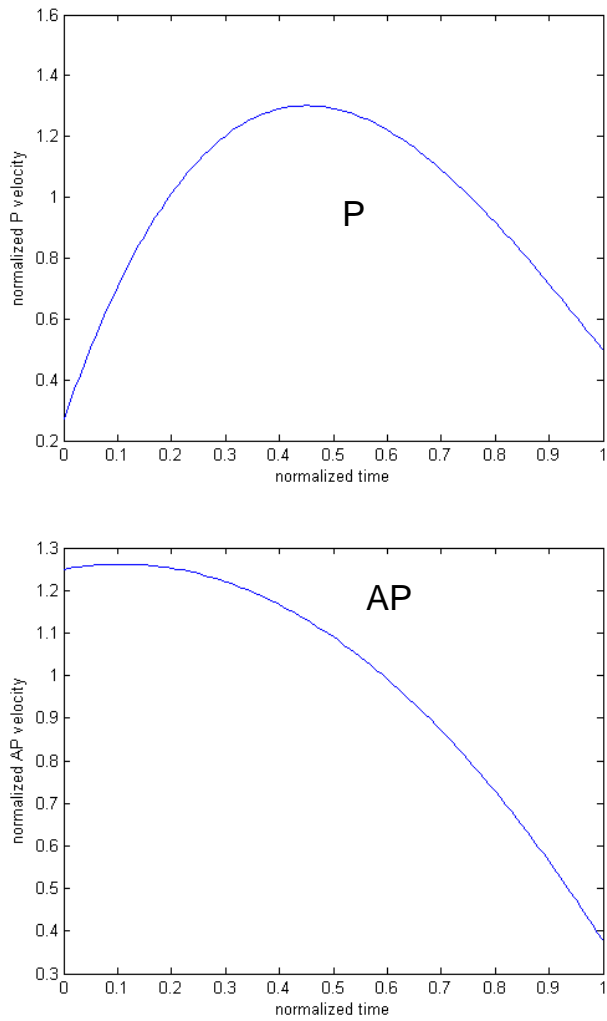


Figure 5.13: Velocities of monopole spindle

Both monopole and bi-pole oscillations show similar velocities pattern for P and AP movement (Figure 5.13). In P motion, leading kinetochore gradually reaches its maximum velocity at middle point of the oscillation and then gradually slows down before it switches direction. In AP motion, kinetochore quickly comes to its top speed and then slows down during most part of the AP movement.

Table 5.2 lists the average velocities and periods in monopole spindles.

	P motion	AP motion
Velocity ($\mu\text{m}/\text{min}$)	1.23 (0.30)	1.09 (0.25)
Period (min)	1.20 (0.32)	1.31 (0.30)

Table 5.2: Monopole velocities and periods

Acknowledgements

I thank Dr. Lisa Cameron and Dr. Daniela Cimini for providing all the live cell images.

CHAPTER 6

K-SHREC

Contributing Authors: Xiaohu Wan, Ryan P O'Quinn, Heather L Pierce, Arshad Desai, E. D. Salmon

Introduction

Kinetochores are protein assemblies at the periphery of centromeric DNA that are required for the segregation of chromosomes in all eukaryotes (Maiato et al., 2004). Robust spindle microtubule plus-end attachment is "end-on" and the microtubules bound to kinetochores are known as kinetochore microtubules (kMTs) (Rieder, 1982). The number of microtubules bound per kinetochore can be as few as one for budding yeast and up to 20 in humans (Maiato et al., 2004; Rieder, 1982). By electron microscopy, human kinetochores show a multilayered disk structure (Dong et al., 2007; Maiato et al., 2004). There is a region at the periphery of centromeric DNA of higher density that is called the inner plate, a low contrast gap of 20-30 nm, an outer plate of 40-50 nm thickness, and a peripheral fibrous corona that extends ~100-200 nm away from the outer plate. Kinetochores with multiple sites for end-on microtubule attachment are assembled from multiple attachment linkages that are aligned side-by-side by weak lateral linkages at the centromere periphery to form the functional kinetochore (Brinkley et al., 1992; Cimini et al., 2004). These observations suggest that the mechanical linkage between centromeric DNA and spindle microtubules is comprised of protein linkages along the inner-outer kinetochore axis.

Here we describe kinetochore architecture in human metaphase cells using a fluorescence microscopy method that we developed termed “Kinetochore-Speckle High Resolution Co-localization (K-SHREC)”. This method is based on a technique developed for measuring separation distances within single molecules (Churchman et al., 2005). We found that K-SHREC is capable of measuring at several nm accuracy the average separations of fluorescent protein markers along the inner-outer axis of sister kinetochores. At metaphase, sister kinetochore pairs exhibit directional instability that produces oscillations in the stretch of the centromeric chromatin in-between sisters (Maiato et al., 2004). Correlating K-SHREC measurements with centromere stretch provided direct information on the stiffness of protein linkages within the kinetochore. We also identify major changes in kinetochore architecture that occur by treating metaphase cells with the MT-stabilizing drug taxol (Waters et al., 1998) which induces spindle checkpoint activation and loss of centromere tension between sister kinetochores without significant loss of bound kMTs (Maiato et al., 2004). Finally, we employed a modified K-SHREC method to locate the positions of the ends of kMTs relative to the microtubule-binding Ndc80 complex. Cumulatively, K-SHREC analysis provides a molecular resolution view of a macromolecular machine with a central role in cell division and reveals the mechanical nature of specific protein linkages at the kinetochore as well as large scale changes in kinetochore architecture induced by suppression of microtubule polymerization dynamics.

Methods

Principles

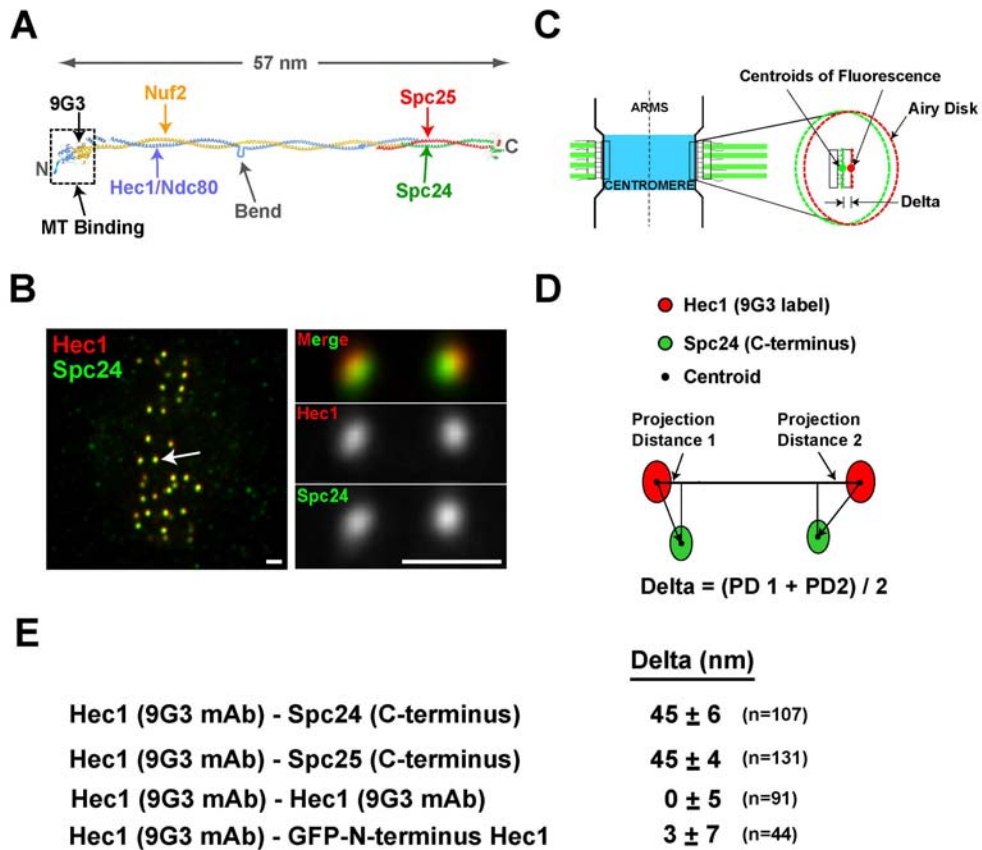


Figure 6.1: K-SHREC principles

We analyzed human kinetochores of metaphase HeLa cells where the kinetochore inner-outer linkages to kMTs are mostly parallel to the axis between sister kinetochores (Figure 6.1 B, C). Two-color immunofluorescence was performed using the 9G3 antibody to Hec1 and polyclonal antibodies to the C-terminal heads of Spc24 or Spc25. We acquired high-resolution, low noise, 3D image stacks of cells where the metaphase spindle was parallel to the coverslip surface—ensuring that several sister kinetochore pairs were in focus within the same optical section and in multiple optical sections (Figure 6.1B). The image in each color is a convolution of the label distribution within the kinetochore and the objective point spread function (Figure 6.1C) (Maddox et al., 2003). As kinetochore proteins are distributed in a layer across the width of the kinetochore (Figure 6.1C), the “Airy Disk” image is elongated into an elliptical cross-section whose major axis defines the orientation of the face of the kinetochore and whose centroid defines the average position of the label along the inner-outer axis of the kinetochore (Figure 6.1C). Sister pairs in or close to the same image plane were selected for analysis. A 3D Gaussian fitting algorithm was used to obtain the 4 centroid coordinates that were needed to calculate the separation of the two color labels, Delta, as depicted in Figure 6.1E. This Delta calculation scheme automatically corrected for the considerable chromatic aberration that prevented direct comparison of the centroids of the two labels at an individual kinetochore—the green label was on average shifted down and to the left of red by about 30 nm, but the exact shift varied with position within the cell. Simulations showed that staggering of attachment site linkages by up to 150 nm along the interkinetochore (K-K) axis (e.g. Figure 6.3D) had little effect on Delta accuracy.

However, tilt of the face of the kinetochore that inclines attachment linkage to the K-K axis (Figure 6.3D) was a source of measurement error (1% in untreated cells) that was corrected to obtain the final average value of Delta.

Centroid Measurement

To obtain the centroids of red and green fluorescent speckle labels at kinetochores of sister pairs, we used nonlinear curve-fitting methods (Chapter 3) that apply to our 3D image stacks least-square curve fitting with a 3D Gaussian function (Thomann et al., 2002). This was accomplished with a customized MATLAB program (Chapter 7) with graphical user interface (GUI) that was developed to make it easy to scroll along the z-axis through the 3D image stacks and identify sister kinetochore pairs near the same plane of focus for semi-automated analysis of the centroid 4 centroid positions, a red and green at each sister. The fitting volume for an individual kinetochore fluorescence was initially set by estimation, typically 7*7 pixels and 5 frames. After the first fitting, the area was adjusted based on size from the fitting results. Then the fitting was performed again under the adjusted area. The 3D Gaussian function reports independent variances for x, y and z dimensions. Rotation transformation was also introduced to the Gaussian function. The independent variances and rotation transformation made the fitting more accurate than simple Gaussian function. The fitting error was approximately 8%. Most kinetochore fluorescence had a peak intensity of 200~400 counts above a low noise background yielding high values for the peak signal to noise ratio, (SNR > 30), (Figure 6.2). That put the accuracy of an individual centroid measurement within less than 5nm (Thomann et al., 2002).

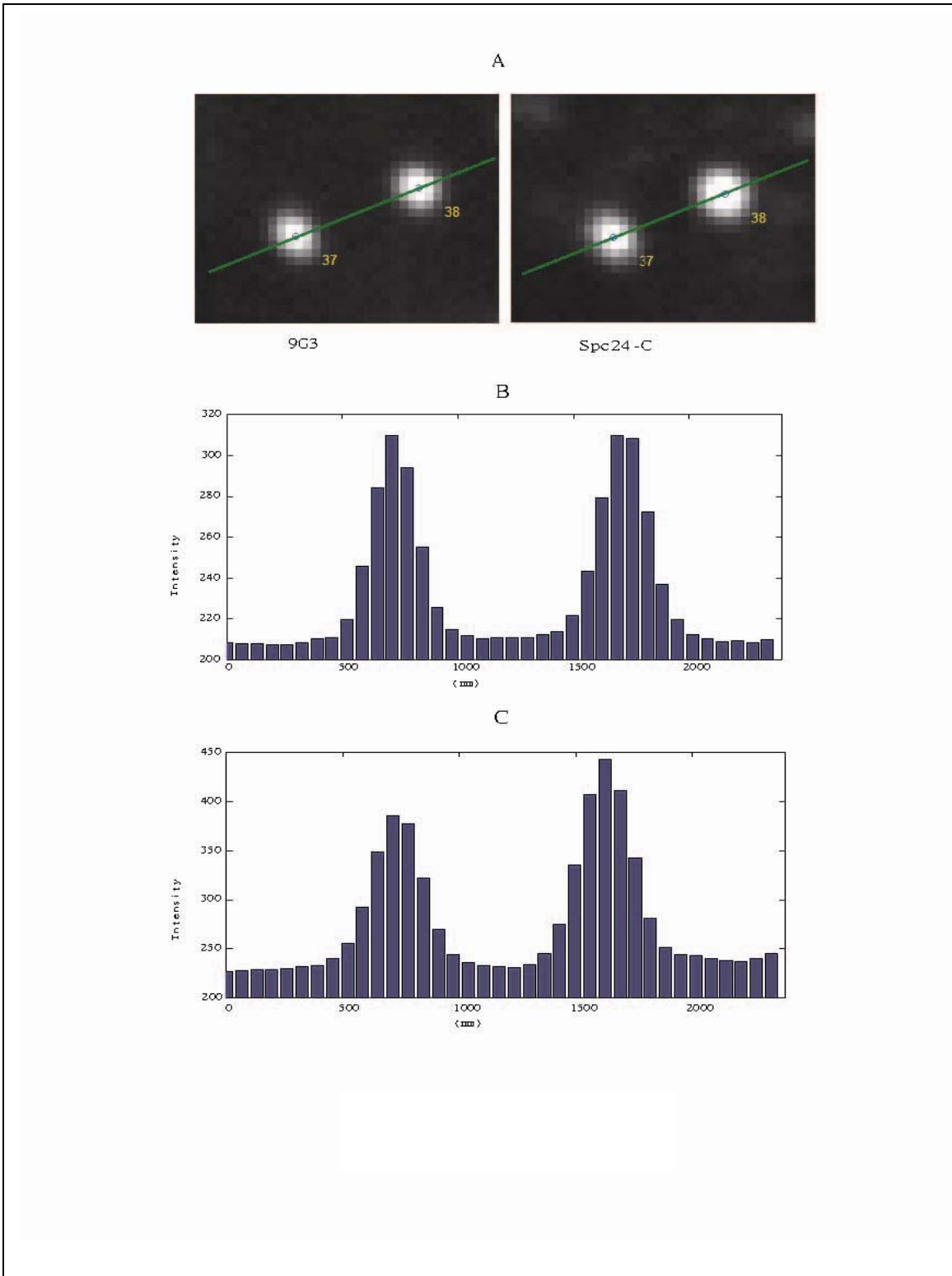


Figure 6.2: Intensity level of kinetochore

Primary Delta Measurement with Chromatic Aberration Correction

In order to correct for chromatic aberrations of the microscope, which can vary between sister kinetochore pairs, the separation distance (Delta) was calculated as an average of a sister kinetochore pair as described in Figure 6.1D, where Delta is calculated from the projections of the mean separation of protein labels within each kinetochore onto the inter-kinetochore axis, which was usually determined by a line through the Hec1 9G3 centroids.

Tilt Correction

Fluorescent speckle images of kinetochores were frequently elliptical in cross-section because the face of the kinetochore was sufficiently wider than the kinetochore depth along the inner-outer axis. They often appeared tilted to the inter-kinetochore axis (Figure 6.1B, Figure 6.3).

The 3D Gaussian function reported the orientations of the major and minor axes of symmetry for each kinetochore fluorescent speckle label. These orientations were used to determine the tilt of the face of the kinetochore, theta (Θ), relative to the inter-kinetochore axis. We found for each kinetochore that the tilt angle for the red fluorescence was always nearly equal to the green fluorescence (Figure 6.3), indicating that all the protein linkages inbetween the red and green labels were oriented in the same way.

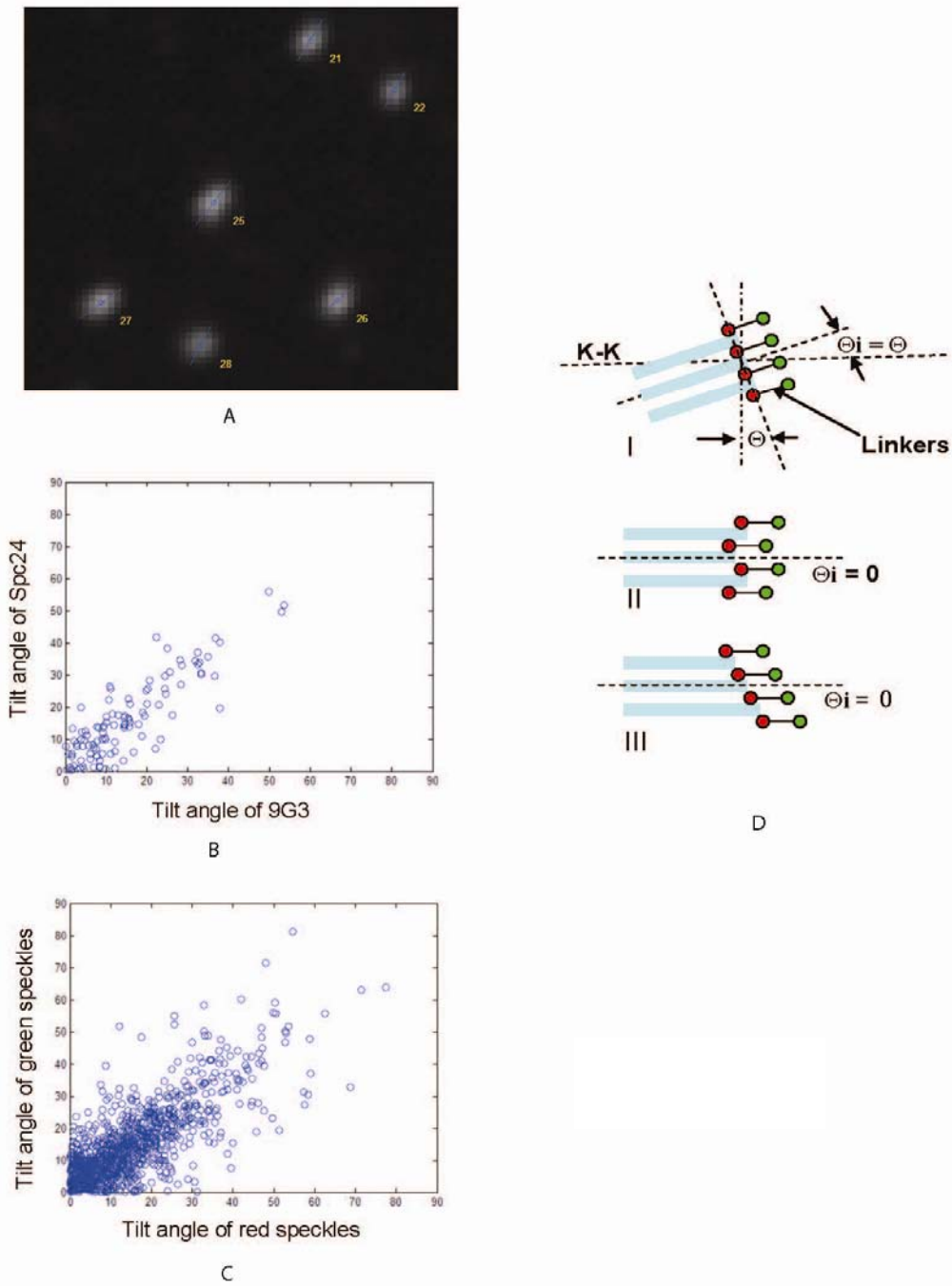


Figure 6.3: Tilt of the kinetochore

The mean value of theta for a sister kinetochore pair was calculated by averaging the four tilt angles, two green tilt angles and two red tilt angles. Each tilt angle was measured by the angle between the perpendicular to the K-K axis and the long axis of the speckle. The orientation of the long axis was obtained from the Gaussian fitting method, which also yielded the dimensions of that speckle. Some speckles appeared round. Some had a more elliptic shape. The orientation of a round speckle was difficult to determine from the fitting method. Therefore, the tilt angles from round speckles were excluded from the tilt analysis. The threshold was set at 1.1 of the ratio between the dimensions of long axis and short axis.

Tilt was a source of error in our Delta measurements only if it was produced by inclination of kMTs and their linkages to the K-K axis (Θ_i in Figure 6.3Di, inclination tilt). On the other hand, tilt of the kinetochore face can be produced when kMTs and their linkages within the kinetochore are parallel to the sister-sister axis, but the kMTs end at different positions as shown in Figure 6.3Diii (sheared tilt). This tilt, nor random differences in the relative positions of kMT ends within untilted kinetochores (Figure 6.3Dii) do not reduce Delta measurements from their true value if the stagger is less than about 75% of the radius of the Airy Disk (~150 nm for green light). This is because the linkages are parallel to each other and parallel to the K-K axis.

To obtain a mean value of Delta for a give pair of fluorescent labels corrected for inclination tilt, we plotted Delta values from sister kinetochore pairs with non-round fluorescent speckle labels verses their mean tilt angle (Figure 6.4). We used least square

fitting of the plots with the function $\text{delta} = A * \cos(\text{Flt} * \text{theta})$, where A is the average Delta value corrected for inclination tilt ($\text{theta} = 0$), and Flt is the average fraction of tilt that is inclination tilt (Figure 6.4, Table 6.1).

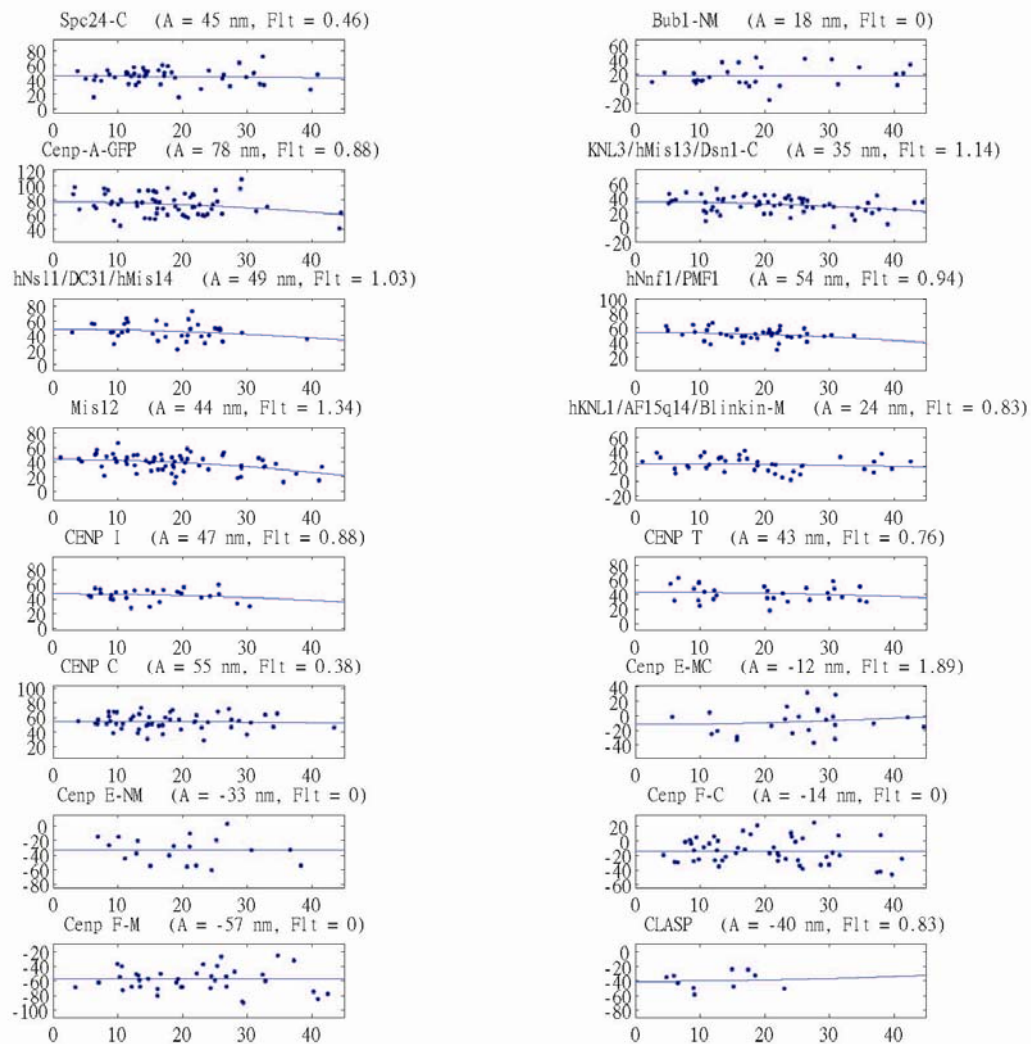
In controls, tilt of the face of the kinetochore occurred with an average $\text{theta} = 15^\circ$, with ~50% of that value due to inclination tilt. This generated only a 1% correction. In taxol treated cells, inclination-tilt was more significant and Delta corrections of as much as 15% were required in a few cases (Table 6.1).

Accuracy

In addition to the tests described for the Ndc80 complex in the Results (Figure 6.1E), for each average Delta value corrected for tilt we obtained the 95% confidence limits about the mean using *ttest* in MATLAB (Table 6.1). We used the *ttest2* function to compare the accuracy of all average value Delta measurements for controls (Figure 6.8). For pairs of average Delta values separated by 3 nm or greater, the probability they were derived from the same data population was $p < .02$.

	Delta_uc	SD	n	SEM	CI (%95 +/-)	A	Fit	Delta	SD	n	Delta - Delta_uc	
control												
Spc24-C	44	7	176	0.5	1	45	0.79	45	6	107	1	
Bub1-NM	27	8	182	0.6	1.2	26	0	26	8	123	-1	
Cenp-A-GFP	105	14	172	1.1	2.2	107	0.49	107	14	116	2	
Spc25	44	4	147	0.3	0.7	45	0.69	45	4	131	1	
KNL3/hMis13/Dsn1-C	46	7	276	0.4	0.8	47	0.62	47	7	159	1	
hNsi1/DC31/hMis14	48	5	97	0.5	1	49	0.84	49	5	80	1	
hNnf1/PMF1	56	6	141	0.5	1.1	56	0.47	56	7	64	0	
Mis12	47	6	149	0.5	0.9	48	0.71	48	6	134	1	
hKNL1/AF15q14/Blinkin-M	34	6	77	0.7	1.4	34	0	34	6	63	0	
CENP I	61	8	115	0.8	1.5	62	0.78	62	7	69	1	
CENP T	59	5	210	0.4	0.7	59	0.59	59	5	120	0	
CENP C	77	10	231	0.6	1.2	77	0.52	77	10	141	0	
Cenp E-MC	-5	18	122	1.6	3.2	-3	0	-3	16	64	-2	
Cenp E-NM	-11	14	209	1	1.9	-13	1.51	-13	15	107	2	
CLASP	-29	9	22	1.9	3.7	-29	0	-29	9	18	0	
9G3 Red vs Green	0	4	117	0.4	0.8	0	0.02	0	5	91	0	
Cenp F-C	-4	10	172	0.7	1.4	-4	0	-4	10	97	0	
Cenp F-M	-46	11	121	1	1.9	-48	0.19	-48	10	54	2	
Hec1-GFP	2	8	121	0.7	1.4	3	-0.01	3	7	44	1	
taxol												
Spc24-C	45	11	167	0.8	1.7	45	0.46	45	11	46	0	
Bub1-NM	17	13	64	1.6	3.2	18	0	18	14	28	1	
Cenp-A-GFP	72	17	129	1.5	2.9	78	0.88	78	15	61	6	
Spc25	44	17	37	2.8	5.5							
KNL3/hMis13/Dsn1-C	30	12	157	1	1.9	35	1.14	35	12	63	5	
hNsi1/DC31/hMis14	42	11	93	1.1	2.2	49	1.03	49	12	35	7	
hNnf1/PMF1	52	9	68	1.1	2.2	54	0.94	54	8	39	2	
Mis12	38	11	111	1	2	44	1.34	44	12	66	6	
hKNL1/AF15q14/Blinkin-M	24	10	93	1	2	24	0.83	24	10	40	0	
CENP I	47	9	83	1	2	47	0.88	47	8	28	0	
CENP T	41	11	140	0.9	1.8	43	0.76	43	11	29	2	
CENP C	54	11	106	1.1	2.2	55	0.38	55	11	51	1	
Cenp E-MC	-8	19	79	2.1	4.2	-12	1.89					
Cenp E-NM	-35	17	63	2.1	4.2	-33	0	-33	18	19	-2	
CLASP	-40	11	11	3.4	6.6	-40	0.83	-40	12	10	0	
Cenp F-C	-14	15	127	1.4	2.7	-14	0	-14	17	50	0	
Cenp F-M	-60	20	98	2	3.9	-57	0	-57	18	39	-3	

Table 6.1: List of measurements



Delta vs theta (taxol)

Figure 6.4: Tilt correction for taxol data

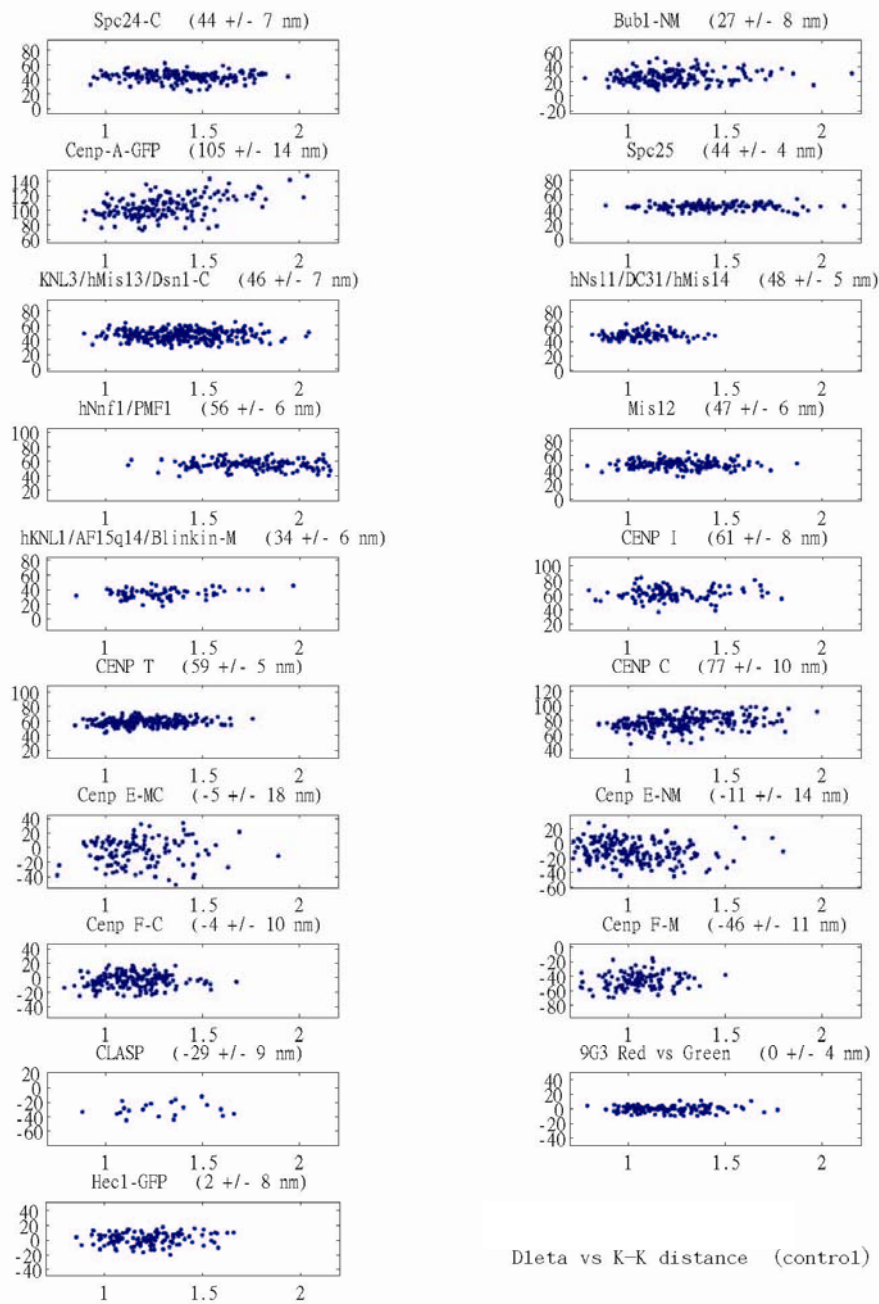
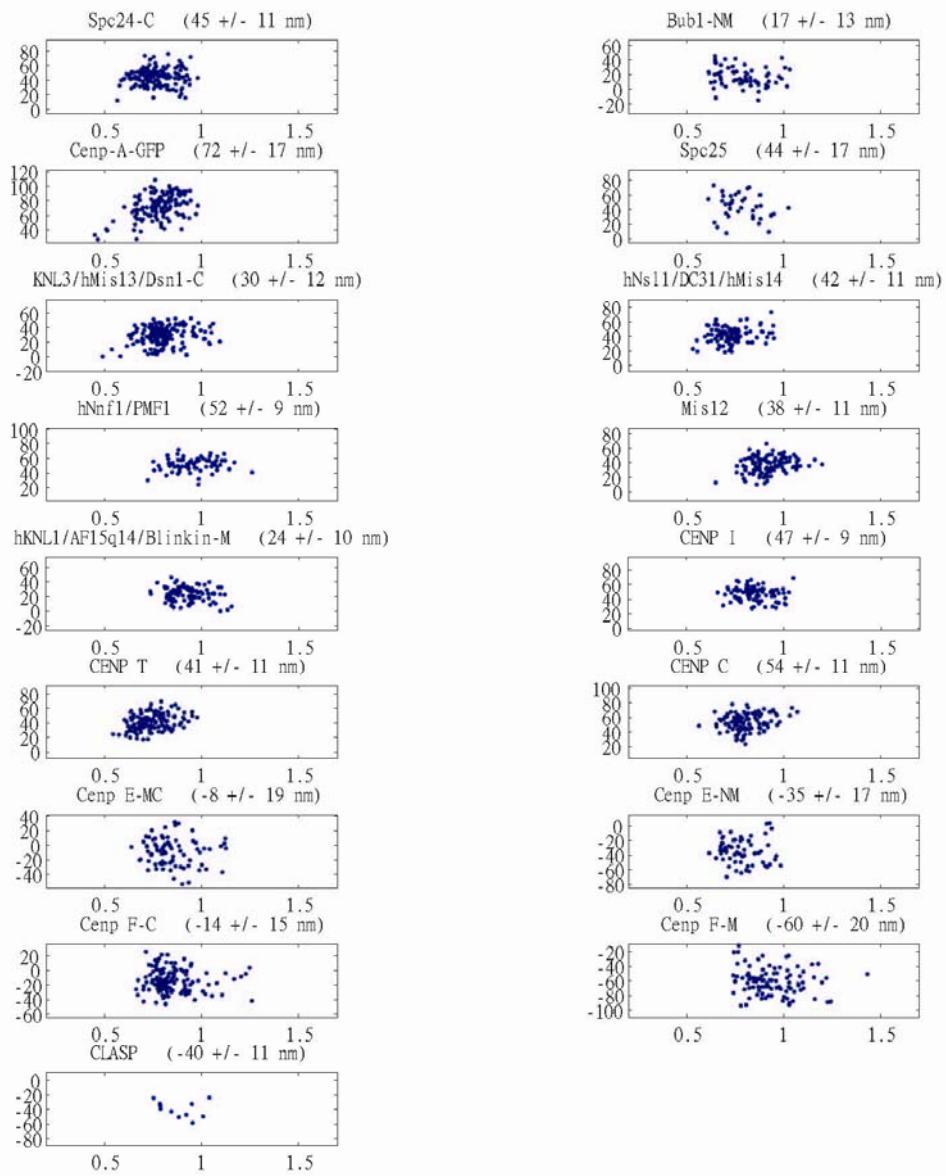


Figure 6.5: Control results



Delta vs K-K distance (taxol)

Figure 6.6: Taxol results

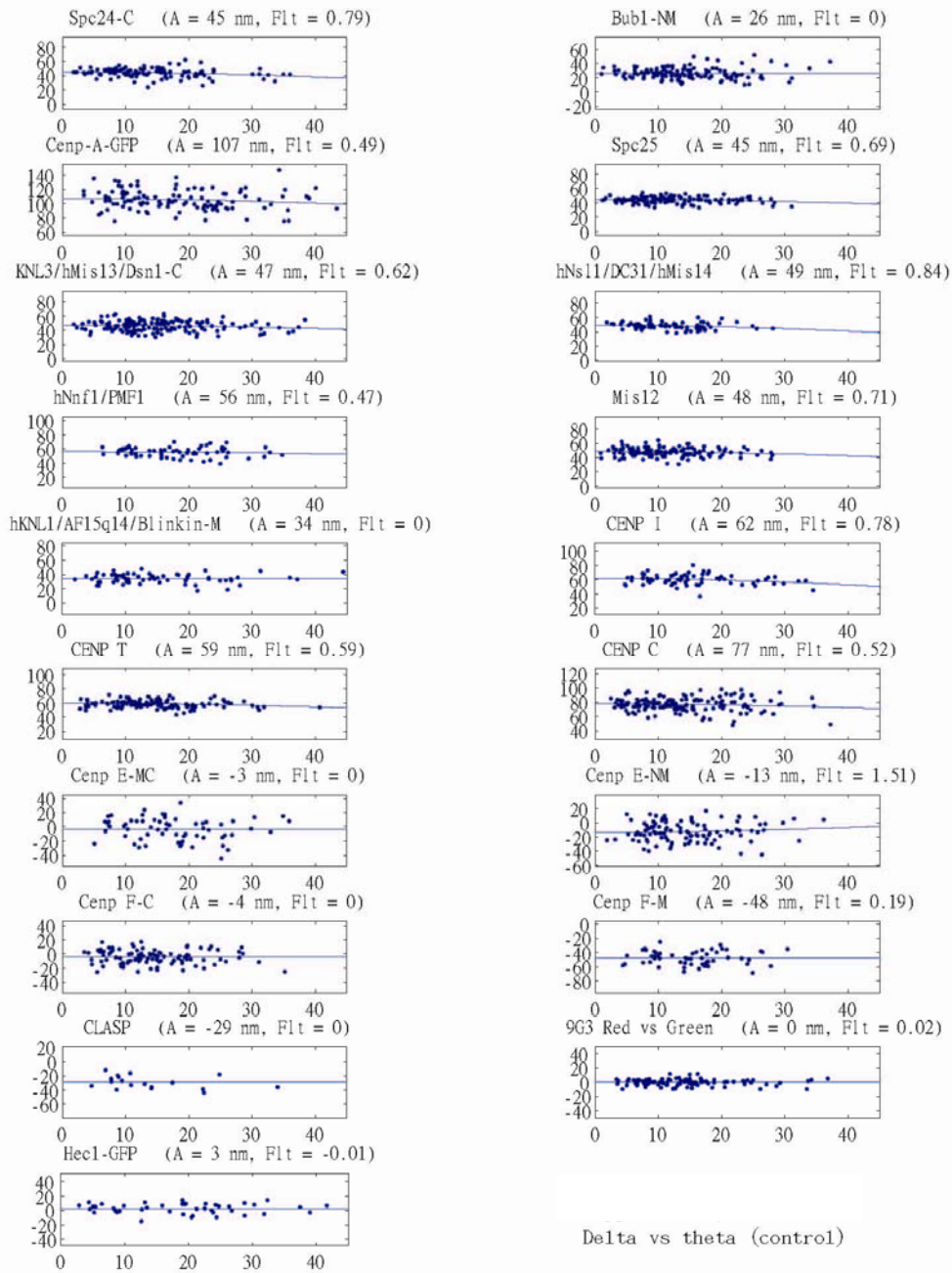


Figure 6.7: Tilt correction for control data

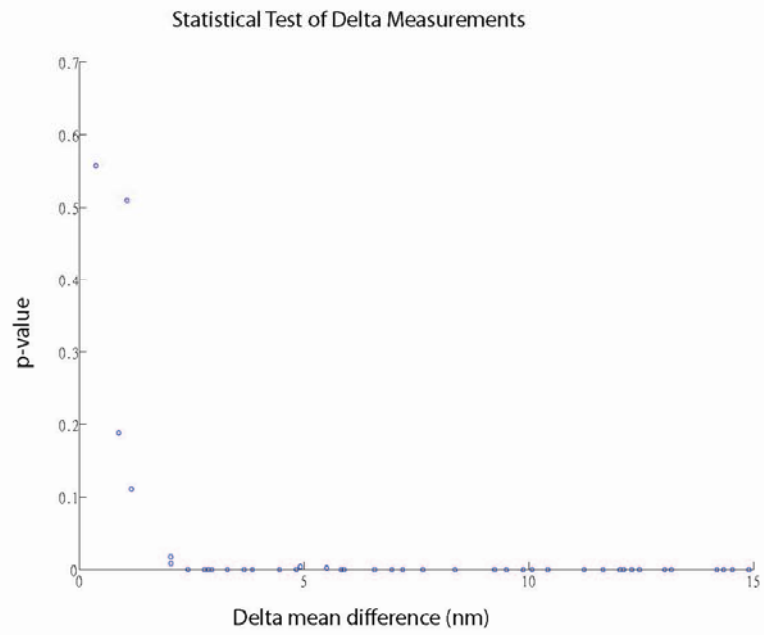


Figure 6.8: Statistical test

Localization of the Kinetochores Microtubule End

For measurements of kMT ends relative to Hec1, PtK2 cells stably transfected with GFP- α -tubulin (Rusan et al, 2001) were used. Linescans were drawn paralleled to the axis of microtubule fibers through the estimated center of the Hec1 fluorescence. The centroid of the Hec1 speckle was then determined through Gaussian fitting. For a bundle of kMTs with ends all occurring at the same position along the central axis of the bundle, its intensity distribution is close to Error function, which is the integration of Gaussian function treated as PSF. The end of such bundle is located at 50% of the maximum intensity level.

All the linescans were normalized on a scale from 0 to 1. Normalized fluorescent intensities for each kMT fiber sampled were plotted together with zero position as the centroid of Hec1. The resulting sigmoid was fit using the equation $y = (1 - \text{erf}((x-a)/b))/2$, with “erf” being the error function. Coefficient “a” when $y=0.5$ is the mean distance in nanometers of the end of kMT fibers from the Hec1 centroid.

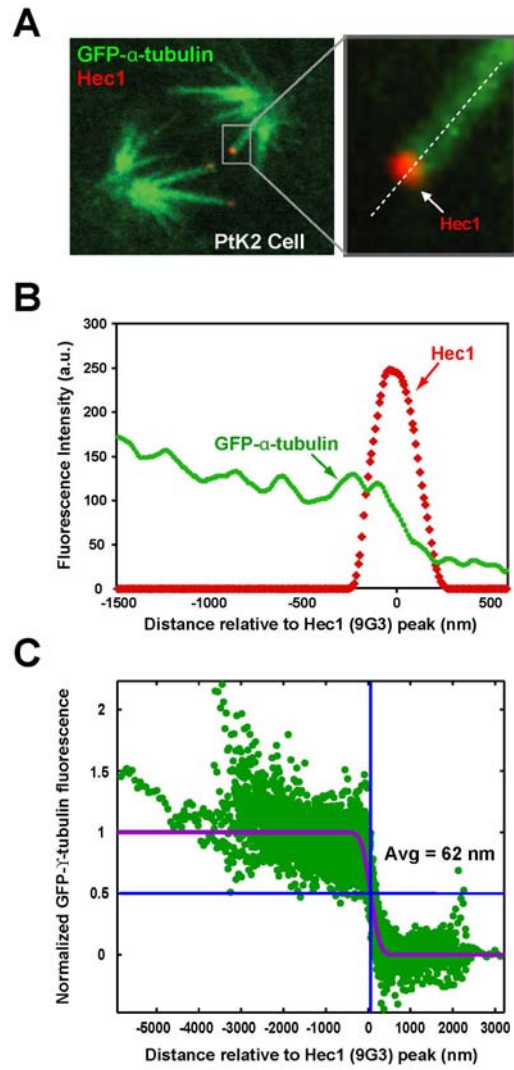


Figure 6.9: MT end measurement

Results

K-SHREC Analysis of the Ndc80 Complex at Human Metaphase Kinetochores

We initially developed the K-SHREC method to analyze the 4-subunit Ndc80 complex, which is the major microtubule-binding component of the outer kinetochore. The Ndc80 complex is 57 nm long and has a dumbbell-shape (Figure 6.1A) (Ciferri et al., 2005; Wei et al., 2005). The 9G3 monoclonal antibody binds adjacent to the Hec1 head (DeLuca et al., 2006) and localizes by immuno-EM to the kinetochore outer plate (DeLuca et al., 2005). Globular C-terminal regions of Spc24 and Spc25 are at the opposite end of a long alpha-helical coiled-coil rod (Figure 6.1A). Previous work has suggested that the 9G3 label is external to the Spc24 label along the inner-outer kinetochore axis (DeLuca et al., 2006).

Using the K-SHREC method, the average Delta value measured between the 9G3 label near the Hec1 head and Spc24 / Spc25 C-terminal antibodies was 45 +/- 7 nm and 45 +/- 4 nm respectively (n= >150 sister kinetochore pairs for each combination). To assess the efficacy of the correction scheme and the accuracy of the K-SHREC method using antibody labeling we labeled Hec1 with the 9G3 monoclonal antibody and used equal amounts of red and green secondary antibodies. The average Delta measured in this case was 0 +/- 4 nm (SD; n= 117 sister kinetochore pairs). As a second test for accuracy, we expressed in HeLa cells Hec1 bound to GFP at its N-terminus and the GFP-Hec1 was incorporated into metaphase kinetochores as expected (DeLuca et al., 2006). The average Delta was 3 +/- 7 nm between fluorescent antibodies labeling GFP and those labeling the 9G3 monoclonal antibody (Table 6.1); a separation expected from atomic

structure to be 5 nm or less (Figure 6.1A) (Ciferri et al., 2008). We also measured in controls the distance between hKnl1-N to Spc25 and to hDsn1 (20 and 22 nm respectively) and compared these to the values obtained for Hec1 9G3 to Spc25 and to hDsn1 (45 nm and 47 nm respectively). Both sets of measurements predicted a 2 nm separation between hDsn1 and Spc25-C. Average Delta values typically had 95% confidence intervals of +/- 1-2 nm (Table 6.1) and two averages that differed by 3 nm or more were significantly different (paired T-test with $p < .02$) because each kinetochore “speckle” image usually had a peak signal-to-noise ratio >30 and we averaged many delta measurements (usually >100) for each label of a sister kinetochore pair. These tests establish K-SHREC as a technique for analyzing kinetochore architecture with an accuracy of several nm and demonstrate that the Ndc80 complex adopts an elongated shape along the inner-outer kinetochore axis whose dimensions are similar to those measured in vitro for the purified complex.

Correlation of K-SHREC Measurements to Centromere Stretch Indicates that the Ndc80 Complex is Non-Compliant

Sister kinetochores of metaphase bioriented chromosomes exhibit directional instability – oscillations characterized by abrupt switches between persistent phases of poleward and anti-poleward movement (Inoue and Salmon, 1995; Maiato et al., 2005; Skibbens et al., 1993). This directional instability produces oscillations in the stretch of the centromeric chromatin interconnecting sister kinetochores. These oscillations are asynchronous between different chromosomes. Consequently, a fixed image of a metaphase cell has within it sister kinetochore pairs that are in different mechanical states (Figure 6.10A). It

is straightforward to assess the mechanical state of each sister pair by measuring the K-K distance using the 9G3 label, which varies during metaphase oscillations between a minimum of ~ 0.8 to a maximum of $\sim 2 \mu\text{m}$ in HeLa cells; the rest length in nocodazole-treated cells is $\sim 0.7 \mu\text{m}$. Thus, correlating Delta values measured using K-SHREC with the inter-kinetochore K-K distance (measured using the 9G3 anti-Hec1 monoclonal) provides direct information on the mechanical properties of the protein linkage reflected by that specific Delta value. The slope of the least-squares line through plots of Delta versus K-K distance represents the stiffness during oscillation of that particular protein linkage at metaphase, which we refer to as the Oscillation Compliance (Figure 6.10A).

When the Delta values measured for the 9G3 and Spc24 antibody labels were plotted as a function of K-K distance, the slope was near zero, indicating that tension changes during sister kinetochore oscillations do not affect the conformation of the Ndc80 complex (Figure 6.10B). The slope was also near zero for data from cells labeled with 9G3 antibody and equal amounts of red and green secondary antibody (Figure 6.10C); a result that shows that Delta measurements were insensitive to K-K separation. We conclude that the Ndc80 complex is a stiff mechanical entity within kinetochores with one end attached to the plus ends of kMTs and the other end located toward the inner kinetochore. These results establish that the Ndc80 complex can be used as a stiff molecular ruler to position other components within the architecture of the kinetochore.

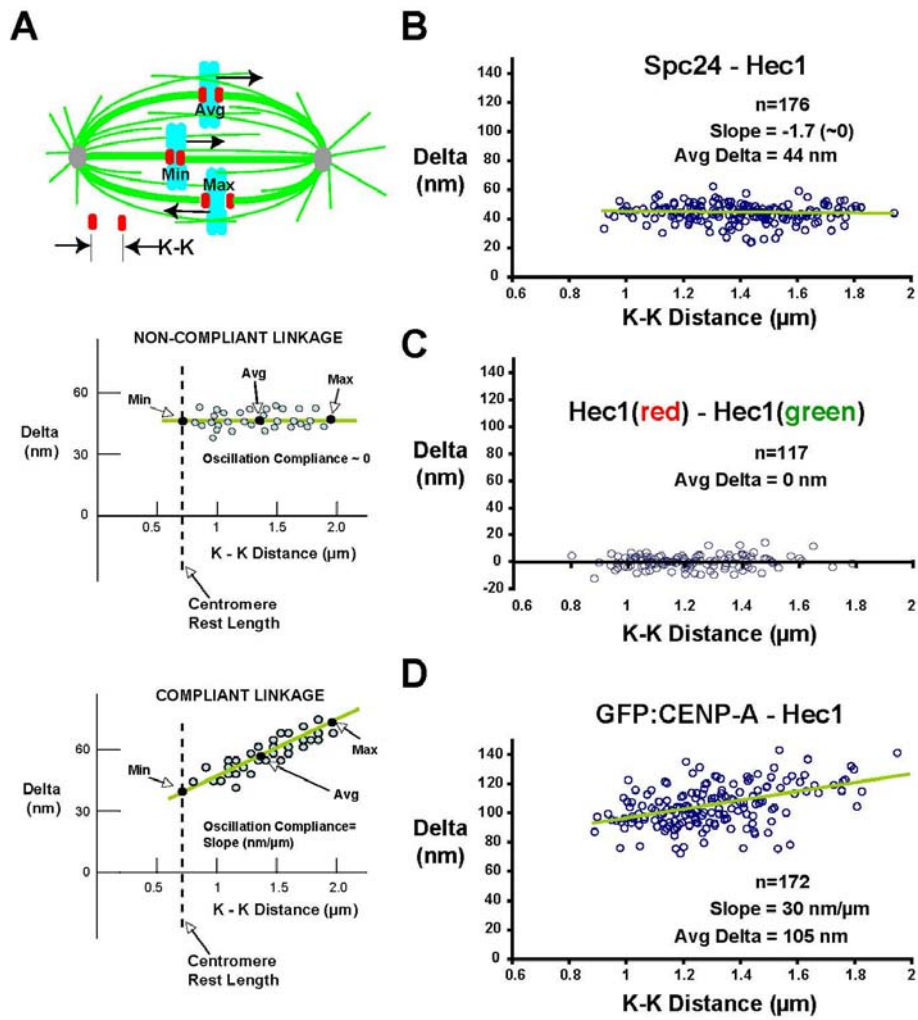


Figure 6.10: Compliance

Human Metaphase Kinetochore Architecture from K-SHREC Analysis of 16 Kinetochore Proteins

We next extended the analysis of position and mechanical properties to 19 epitopes in 16 proteins representing all of the distinct groups comprising core kinetochore structure. For three of the analyzed proteins that are very large (hKNL1, CENP-E and CENP-F), we analyzed two different regions using independent antibodies. The entire dataset is summarized in Figure 6.11; the positions along the kinetochore inner-outer axis for all the protein epitopes we have measured by K-SHREC are plotted relative to the 9G3 anti-Hec1 monoclonal antibody. Positive values are outside (i.e., towards the spindle side) of the position of the 9G3 centroid and negative values are inside (i.e., towards the centromeric DNA). All average Delta values in this position map have been corrected for inclination-tilt (Figure 6.3; Table 6.1). The data for control cells is on the left with dots indicating average values. The mechanical properties of each Delta value are summarized by vertical lines through the average dots which indicate minimum to maximum variation with K-K separation. The average position data for taxol-treated cells is on the right and the insights derived from this perturbation are discussed in the next results section. With this overview of the entire K-SHREC dataset, we describe specific aspects of the measurements for each protein/protein complex.

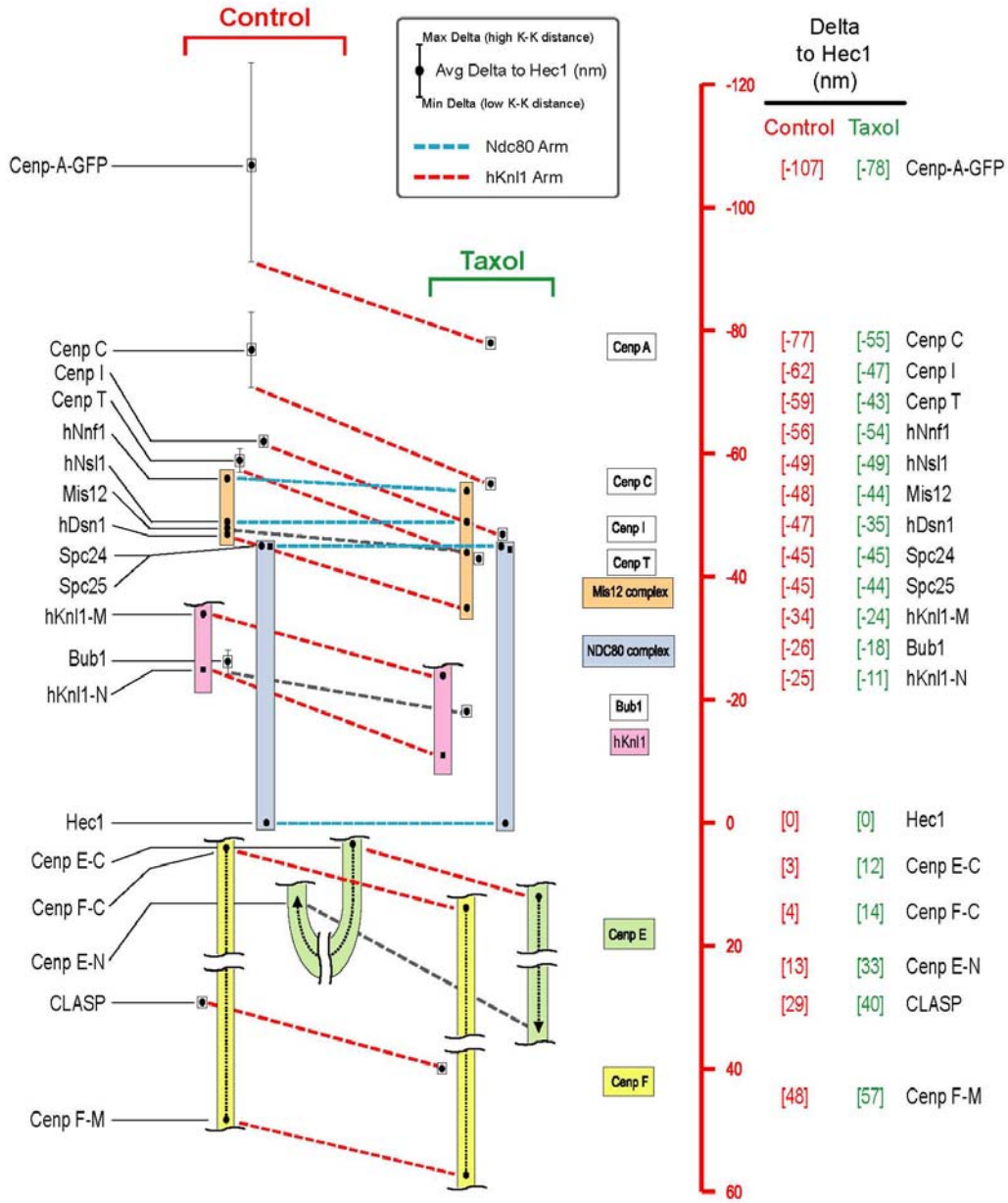


Figure 6.11: Protein map

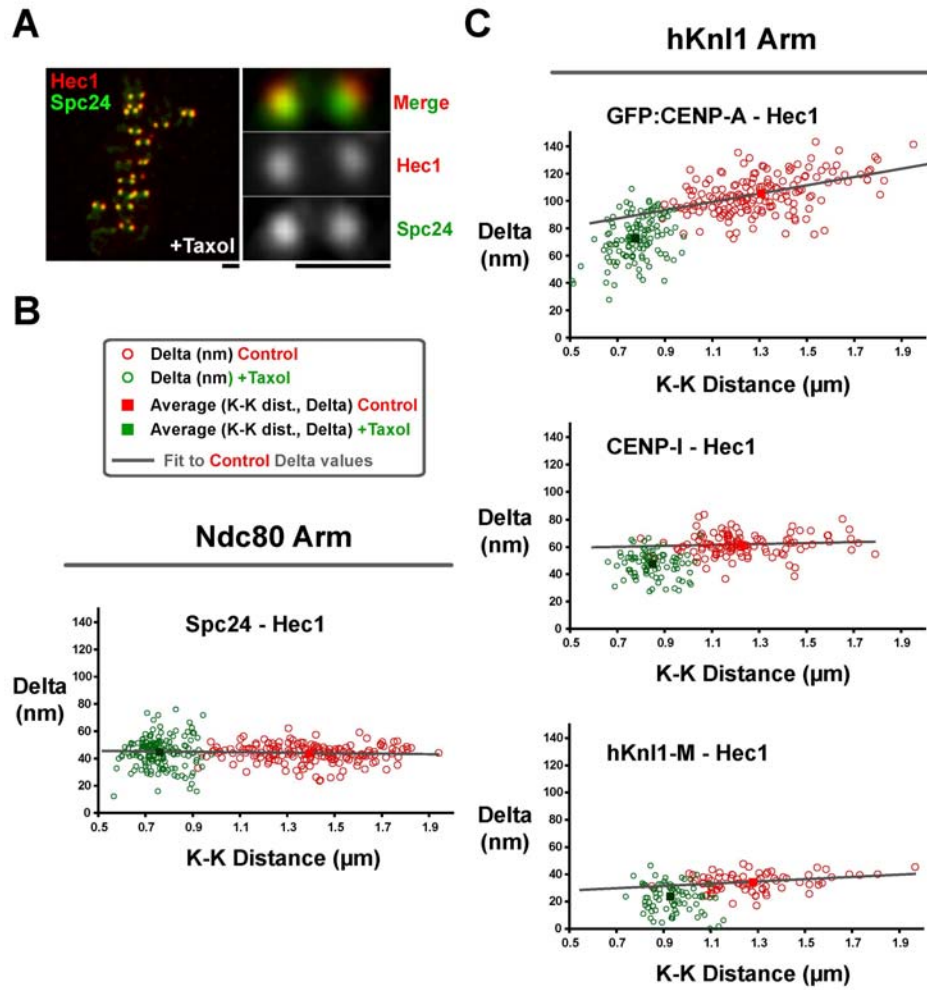


Figure 6.12: Control and taxol results

I. Constitutive Centromere-Associated Proteins

CENP-A and CENP-C

The centromeric histone H3 variant CENP-A and the closely associated conserved CENP-C protein are present at centromeres throughout the cell cycle and provide a foundation for kinetochore assembly. In control cells, average Delta of CENP-A-GFP relative to the Hec1 head was 107 nm and there was a pronounced upward slope of Delta with centromere stretch (increased K-K distance) (Figure 6.10D, 6.12). The average Delta for CENP-C, which has direct DNA binding activity (Politi et al., 2002) and lacks extended coiled-coils, was 77 nm and the oscillation compliance was ~40% of that exhibited by CENP-A (Figure 6.12). From the entire set of proteins analyzed by K-SHREC (Figure 6.12), these were the only two proteins that exhibited significant oscillation compliance relative to the Ndc80 complex.

CENP-I and CENP-T

In addition to CENP-A and CENP-C, 13 additional constitutive centromere-associated network (CCAN) proteins (CENP-H, -I and -K to -U) localize to centromeres throughout the cell cycle and play important roles in chromosome segregation (Foltz et al., 2006; Hori et al., 2008; Okada et al., 2006). In control cells, the average positions of CENP-I and CENP-T were about 17 and 14 nm inside the Spc24/Spc25 end of the Ndc80 complex, respectively (Figure 6.11). In contrast to CENP-A and CENP-C, CENP-I and CENP-T did not exhibit any oscillation compliance (Figure 6.11, Figure 6.12C, Figure 6.4). This result suggests that components of the CCAN (excluding CENP-C) assemble in the 34 nm gap between the centroid of CENP-C and the Spc24/Spc25 end of the Ndc80 complex and they exhibit a stiff linkage to the Ndc80 complex during oscillations.

II. The KMN Network and the Spindle Checkpoint Kinase Bub1

The KNL1/Mis12 Complex/Ndc80 Complex (KMN) proteins play a central role in kinetochore architecture and in microtubule binding. As described above, the two ends of the Ndc80 complex are ~45 nm apart and this complex appeared stiff with no oscillation compliance (Figure 6.10B). The 4 subunits of the Mis12 complex extend from the Spc24/25 end of the Ndc80 complex to about 9 nm inside it, next to the centroid of CENP-T (Figure 6.11) and also do not exhibit oscillation compliance. We measured the position of the central region of hKnl1 using an antibody to amino acids 1220-1440 and the position of the N-terminus using a monoclonal antibody to the first 43 amino acids. These epitopes were found to be on average 34 nm and 25 nm inside from the Hec1 head (Figure 6.11) and neither exhibited significant oscillation compliance.

An antibody to Bub1 raised to a region near its kinetochore-targeting domain was 26 nm internal to the Hec1 head and just inside of the N-terminal epitope in hKnl1 (Figure 6.11). The distance between hDsn1, a likely marker for the C-terminal region of hKnl1 (Cheeseman et al., 2008; Kiyomitsu et al., 2007) and the N-terminus of hKnl1 was a constant 21-23 nm across the entire range of K-K distances indicating a lack of oscillation compliance (Figure 6.4, Table 6.1). This result indicates that hKnl1 is stiff like the Ndc80 complex and that its long axis is oriented primarily along the inner-outer axis of the kinetochore.

III. Corona Proteins

The Motor CENP-E

CENP-E is a plus-end directed dimeric motor protein, with a very long (225 nm) coiled-coil stalk and a globular tail domain (Kim et al., 2008). We found that the centroid of an antibody to amino acids 1571-1859, about 100 nm from the C-terminal kinetochore-targeting domain was about 4 nm outside of the Hec1 head (Figure 6.11). Surprisingly, the centroid of an antibody to amino acids 663-973, about 50 nm from the motor domain of CENP-E, was only ~13 nm outside the Hec1 head. Neither epitope on CENP-E exhibited any oscillation compliance (Figure 6.4, Figure 6.11). This result indicates that the 225-nm long CENP-E molecule is bent with both its tail and motor domains located near the Hec1/Nuf2 heads.

The Coiled-Coil Protein CENP-F

CENP-F is a major component of the fibrous corona as determined by immunogold EM (Rattner et al., 1993). It is large (300kD, 3210aa) and dominated by extensive central alpha helical coiled-coil domains. An antibody to the C-terminal 561 aa localized ~5 nm outside the Hec1 head, and a different antibody to a region in the middle of the molecule (Figure 6.11) was ~45 nm outside the Hec1 head, indicating that CENP-F is primarily oriented perpendicular to the outer plate.

The Microtubule Polymerization-Promoting Protein CLASP

CLASP is a microtubule-binding protein that promotes polymerization, suppresses depolymerization, and concentrates at the growing tips of microtubules in the cytoplasm of interphase cells (Maiato et al., 2005). CLASP is concentrated within the very periphery of the kinetochore during mitosis. We find that the centroid of CLASP is 29 nm outside of the Hec1 head in control metaphase cells (Figure 6.11).

Large Changes in Kinetochores Protein Architecture Are Observed Following Taxol Treatment

The anti-cancer agent taxol suppresses the polymerization dynamics of microtubules. Taxol treatment eliminates the tension at metaphase kinetochores and activates the spindle checkpoint. The mean inter-kinetochore distance in taxol-treated metaphase cells is about 0.75 μm (Figure 6.4A), only slightly less than the minimum 0.8 μm value that transiently occurs during oscillations (Figure 6.10). This similarity would suggest that K-SHREC measurements under taxol treatment should resemble the values observed at lowest K-K distance for linkages with oscillation compliance (CENP-A and CENP-C) and similar to the average values for the stiff non-compliant linkages. Consistent with this, the dimensions of the stiff Ndc80 complex remained constant in taxol (Figure 6.11, 6.12B). However, somewhat surprisingly, there were several significant changes induced in the architecture of the kinetochore in taxol-treated cells. The centroids of CENP-A, CENP-C, CENP-I, and CENP-T all moved about 12 nm closer to the position of the Spc24/25 end of the Ndc80 complex (Figure 6.11, 6.12C). This movement did not change the relative separation distance between CENP-I and CENP-T centroids that do not exhibit oscillation compliance. In addition, the separation between CENP-I - CENP-C centroids and CENP-I - CENP-A centroids was the same as that observed at minimal centromere stretch (K-K distance) during normal control oscillations. Thus, the entire inner kinetochore is ~ 12 nm closer to the Spc24/25 end of the Ndc80 complex in taxol-treated cells.

The Mis12 complex also exhibited a striking change in taxol-treated cells (Figure 6.11). In control cells, the distance along the inner-outer axis from the hNsl1 subunit at the interior end of the Mis12 complex and the hDsn1 subunit at the exterior end was constant at about 9 nm; in taxol this length became 19 nm. Two components at one end of this elongated complex, hNnf1, and hNsl1/Mis14 did not significantly change their position relative to Spc24 after taxol treatment; Mis12 showed modest (4 nm) outward movement. In contrast, a striking effect was observed for hDsn1, which shifted ~12 nm outward in taxol-treated cells.

hDsn1 likely directly binds to the C-terminal region of hKnl1 (Kiyomitsu et al., 2007); consistent with this, hKnl1 also exhibited outward movement of similar magnitude to hDsn1. The centroid of the Bub1 epitope also moved outward, but less than expected for its putative binding location near the N-terminus of hKnl1; this lack of movement might indicate a change in Bub1 binding sites following taxol treatment.

The C-terminal regions of the large corona proteins CENP-E and CENP-F also moved ~11 nm outward relative to the Hec1/Nuf2 heads after taxol treatment (Figure 6.12). The most striking change observed in the corona was in the motor CENP-E: the epitope close to the motor domain moved from near the Hec1 head (and its own C-terminus) in controls to 33 nm beyond the Hec1 head. This result suggests that CENP-E changes from a bent conformation in control metaphase cells to an extended conformation in taxol-treated cells.

A major pattern emerging from comparison of the taxol-treated and control cell K-SHREC measurements suggests relative movement of two protein sets whose constituents behave as if they are coupled and move together – we refer to each of these protein sets as an “arm” in order to connote a multi-part mechanical entity. The Ndc80 arm (whose average Delta values are linked using blue dotted lines between control and taxol treatment in Figure 6.11) is comprised of the Ndc80 complex and the hNnf1, hNsl1 and part of Mis12—none of these show significant taxol-specific changes in separation. The hKn11 arm (whose average Delta values are linked using red dotted lines between control and taxol-treatment in Figure 6.11) is comprised of CENP-A, CENP-C, CENP-I, CENP-T, the hDsn1 and part of the Mis12 subunits, hKn11, Bub1, CENP-F, and the C-terminal end of CENP-E – all of these move ~10-12 nm outward relative to the Hec-1 head (for the compliant CENP-A and CENP-C linkages, this movement is relative to the Delta value measured at minimal K-K distance, i.e. lowest tension state in control cells—see point where lines linking the control and taxol data sets are drawn). As the distance between the centromeric inner kinetochore proteins (e.g. CENP-I/CENP-T) and proteins in the Ndc80 arm decreases in taxol-treated cells, we conclude that the Ndc80 arm moves in towards the centromeric chromatin in taxol-treated cells whereas the hKn11 arm does not. This shift, which is not observed at minimal K-K distance in control cells, suggests the existence of a mechanism in taxol-treated cells that leads to uncoupling and relative movement of these normally coupled protein arms.

In summary, taxol treatment did not recapitulate kinetochore architecture at lowest K-K distance but instead revealed large-scale changes in different regions of the kinetochore.

These changes may arise from persistent absence of mechanical tension (as opposed to the transient absence in oscillating kinetochores), the activation of the spindle checkpoint, or both.

Location of the Plus Ends of Kinetochores Microtubules Relative to the Ndc80 Complex

The average position of the microtubule end determined using this method was 63 +/- 15 nm inside of the centroid position of the 9G3 label (Figure 6.9C). The variance is large because fibers oriented at different angles within the field of view have different amounts of lateral chromatic aberration. These results indicate that, on average at 6°C in PtK2 cells, the plus ends of kMTs extend 10-15 nm inside the Spc24/Spc25 ends of the Ndc80 complexes. In taxol-treated cells, this position would be at the periphery of the inner centromere.

Orientation of Kinetochores Plate Is Not Related to the Kinetochores Microtubules

Kinetochores microtubules are generally considered in the perpendicular position to the kinetochores plate. In our study, we found that this is not true. Spindle in HeLa cell is organized in a way that the angle between kMTs and metaphase plate decreases gradually from the center of the spindle to the peripheral of the spindle (Figure 6.9A). At the center, the angle is almost 90 degree. At the edge of the spindle, it becomes around 60 degree. kMT angle to the metaphase plate is correlated with its position to the spindle. The angle decreases when it is away from the center and increases when it is close to the center.

If kinetochore microtubules are always perpendicular to the kinetochore plate that they are attached to, the angle of the kinetochore plate (tilt angle) should also be correlated to the position within the spindle. The closer to the spindle center, the smaller the tilt angle should be. Further away to the spindle center, greater such angle should become.

However, in our study, the angle is not correlated with the position in the spindle. It is randomly distributed. This implies that attachment angle between kMT and kinetochore plate is also randomly distributed along the spindle. They range from 0 to 30 degree.

Kinetochore Becomes Deformed under the Treatment of Nocodazole

Nocodazole stops the polymerization of microtubule. When cell is treated with nocodazole, kinetochore loses its microtubule attachment. Figure 6.13 shows the deformation of the kinetochores. Delta measurement shows that distance between 9G3 and Spc24-C becomes shorter compared the results in taxol.

Curved kinetochore images (Figure 6.15) were simulated by convolving PSF and curvature of the kinetochore plate (Figure 6.14). Green and red PSF were used to generate red and green speckles. Delta measurement from the simulation images demonstrates that curvature shortens the distance between the red and green labels. The more kinetochore is curved, or, the smaller radius the curvature has, the shorter Delta will be (Figure 6.16).

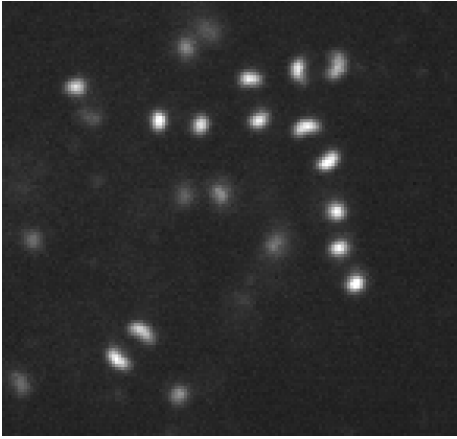


Figure 6.13: Kinetochores from nocodazole treated cells

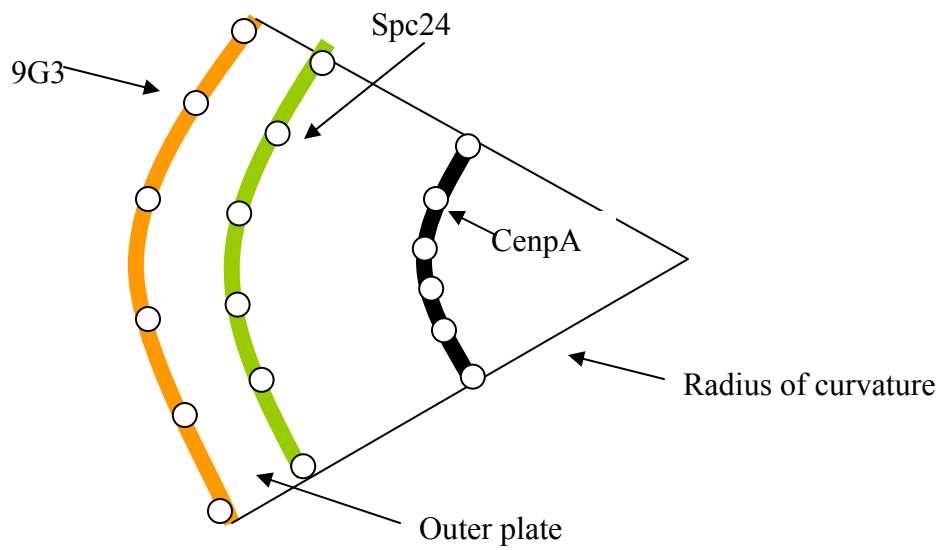
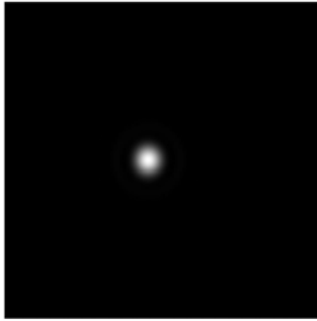
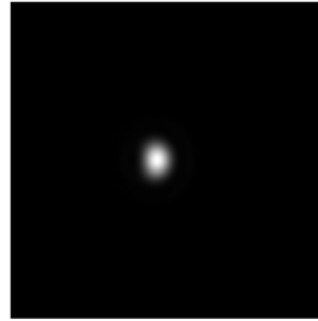


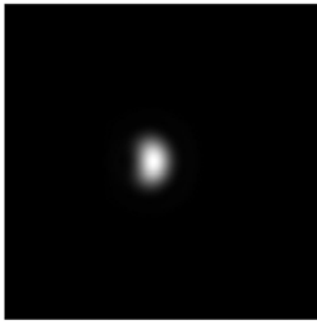
Figure 6.14: Curvature of kinetochore



CenpA



Spc24



Hec1

Figure 6.15: Simulated kinetochore images

The Delta value between Spc24 and 9G3 in nocodazole is 19 nm. For CenpA, the value is 34 nm. Based on the simulation results, both measurements suggest that the radius of curvature is 150nm (Figure 6.16). This may imply that the inner plate and the outer plate are curved or bended together in the same way. All the nocodazole measurements in this study are listed in Table 6.2.

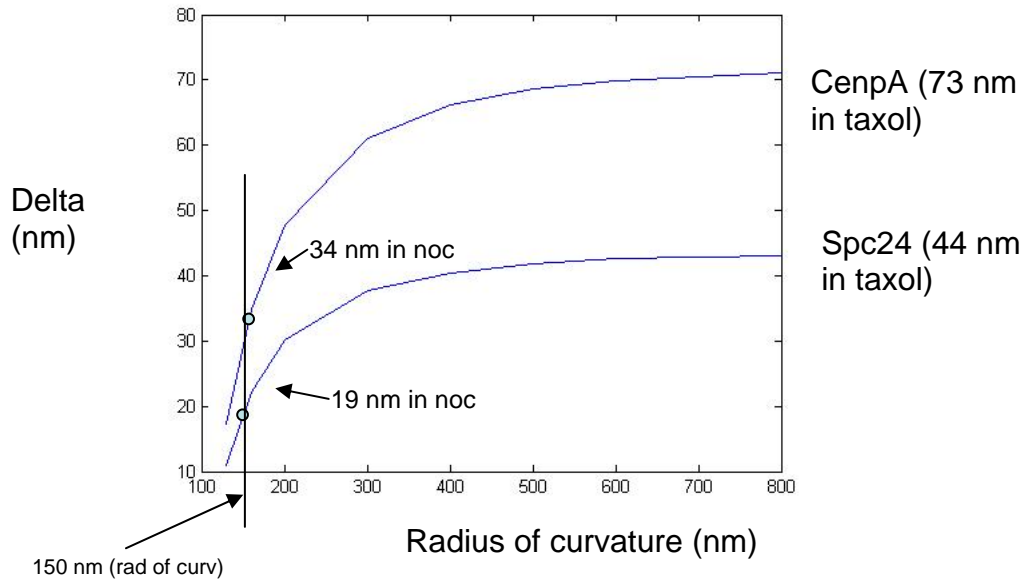


Figure 6.16: Curvature and Delta

Delta to 9G3 (nm)

spc24	19
CenpA GFP	34
CenpA Ab	23
spc25	17
KNL3/hMis13/Dsn1-C	-3
hNsl1/DC31/hMis14	11

Table 6.2: Nocodazole measurements

Acknowledgements

We thank Dr. Steve Taylor, Dr. Mitsuhiro Yanagida, Dr. Tomomi Kiyomitsu, Dr. Aaron Straight, Dr. Jan Ellenberg, Dr. Kerry Bloom, Dr. Andrea Musacchio, Dr. Ajit P Joglekar,

Dr. Walt E Gall, Dr. Jennifer G DeLuca, Dr. Christopher W Carroll, Dr. Song-Tao Liu
and Dr. Tim J Yen for providing critical antibodies and helpful discussions.

CHAPTER 7

SOFTWARE DEVELOPMENT

Introduction

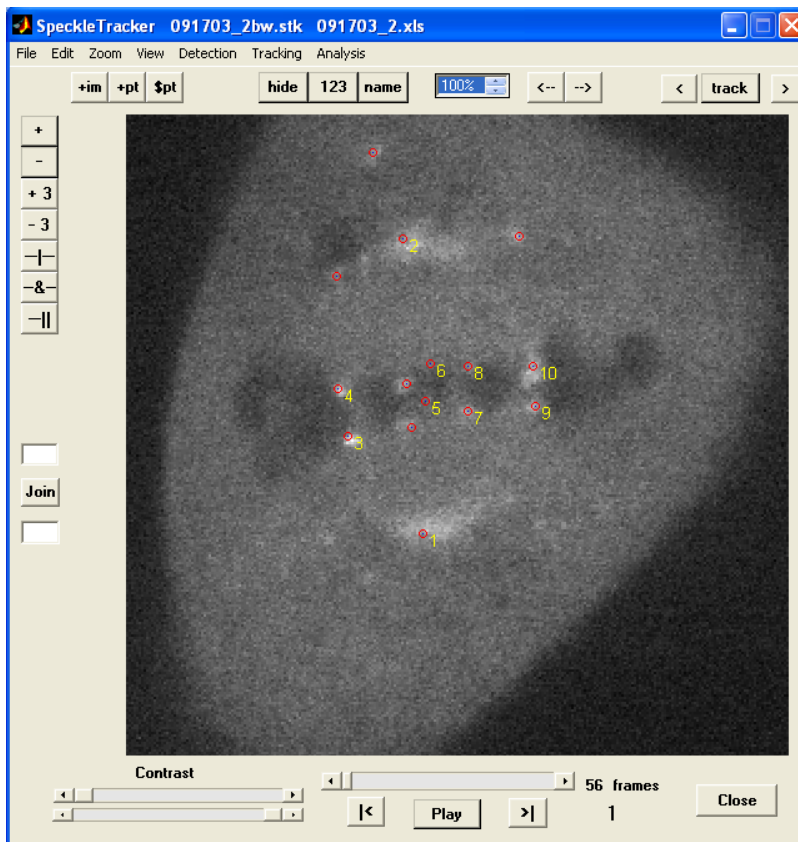


Figure 7.1 SpeckleTracker

In biological research, studying and analyzing microscopy imaging plays an essential role in understanding how a cell works. Analyzing image data often involves object identification. Because biological data tend to have large volume, identifying objects of interests can be a time-consuming process for researchers and prone to human errors.

SpeckleTracker is a software program designed for studying the movement and localization of speckles, especially those of the kinetochores. It was developed with the MATLAB program and its graphical user interface (GUI) (Figure 7.1). It has speckle detection, tracking, editing and analysis functions.

Software design

The purpose of designing SpeckleTracker software was to study the localization and movement of speckles, mainly kinetochores. The majority of the images used in the dissertation study were acquired from Metamorph (Molecular Devices, Sunnyvale, CA) software. SpeckleTracker was designed to deal with images with Metamorph “.stk” format. It can open and display Metamorph “.stk” image files.

Data structure

Two kinds of data are central to the design. One is the data for the images. The other is the data for the speckles. All the functions in the software including image display, speckle detection, tracking, editing and analysis focus around those two data types. Object-oriented programming method was adapted. Two classes were used to present the two data types. One is called “ImageClass”. The other is called “PointClass”.

Interface

Program interface (Figure 7.2) was design under MATLAB GUIDE (Graphical User Interface development environment), Figure 7.2. A common layout about menu, button and display is used.

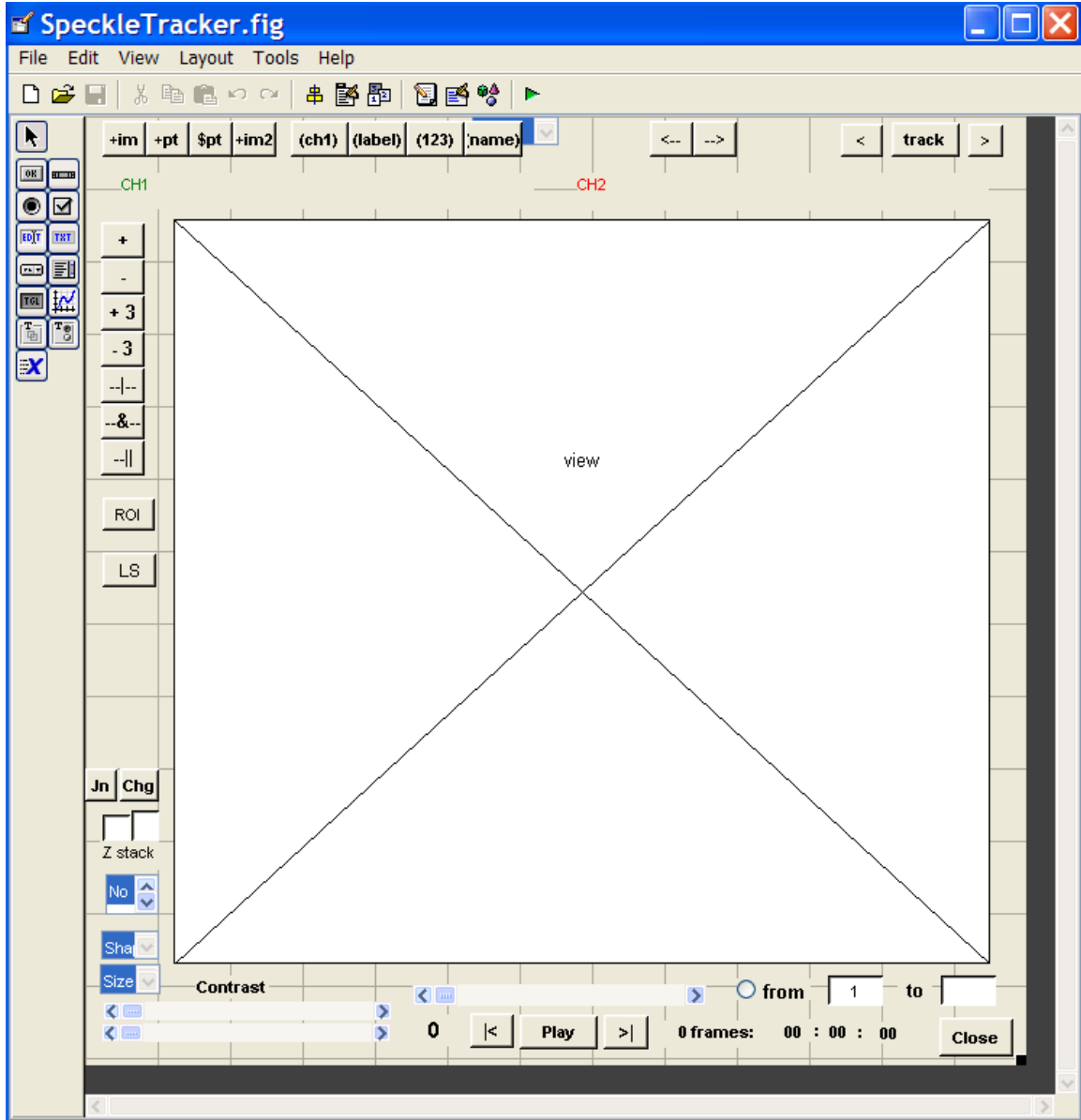


Figure 7.2: Interface design

Software functions and instructions

Open image files

The function used in opening Metamorph image file is a MATLAB routine developed by EMBL (the European Molecular Biology Laboratory). The image data is saved in “ImageClass”. To open a single image file, click on “open stack” from “file” menu, or click on “+im” button (Figure 7.3).

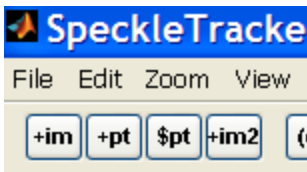
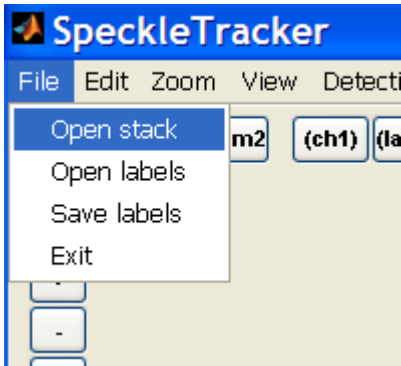


Figure 7.3: Open image

Click on the “+im2” button to open the second image. When two images are opened, the first one is always regarded as green channel and second one is always treated as red channel.

Display and adjust image

After the image file is opened, specklertracker will display it in the center of the program (Figure 7.4). Because of contrast, the image may not display properly at first. The

contrast can be adjusted by the viewers using the two contrast bars at the bottom of the interface (Figure 7.4, 7.5). Contrast can be independently adjusted for each color channel of color image.

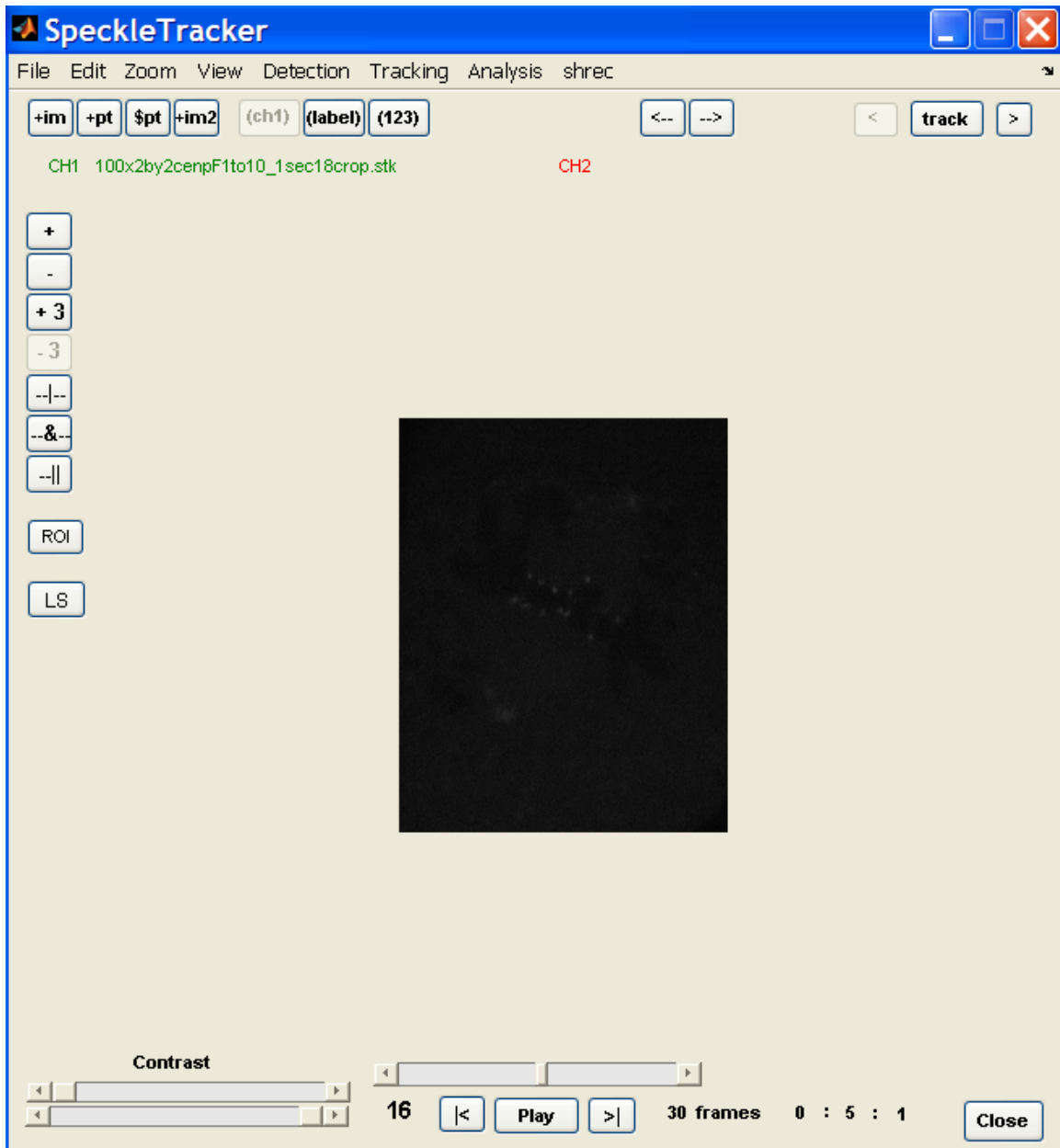


Figure 7.4: Image display



Figure 7.5: Adjust contrast

Click on the “Play” button to play the whole image sequence. Click on the same button (appearing “stop” after image played) one more time, the movie will stop. Clicking on “|<” and “>|” buttons will display the first and last frame of the stack. Use the frame bar or left/right arrow keys to go over individual frames.

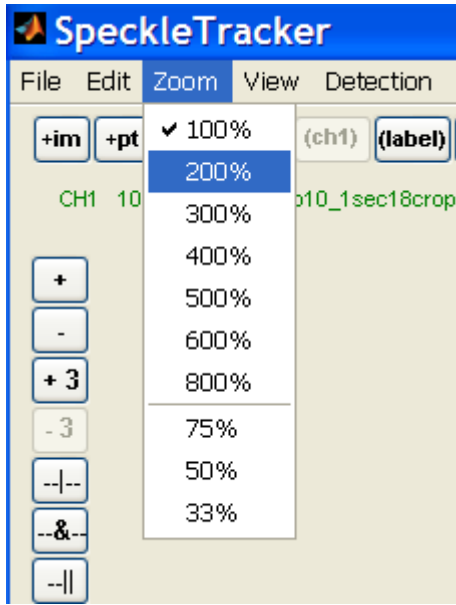


Figure 7.6: Zoom

To zoom the image, use either “zoom” menu (Figure 7.6) to select how much you want to zoom and click on the image to select zoom center. The zoomed image will display after the click.

When two images of red and green channels are opened, using “ch1” button can switch among different display modes: display green image only, display red image only and display color combined image.

Display labels for speckles

SpeckleTracker can also read coordinates file (excel file) generated by Metamorph and display the coordinates over the image. This feature allows users to review the positions of speckle labels done from Metamorph and adjust them. The label is shown as a red circle over the speckle (Figure 7.1). It shows the exact position of that speckle. Some

labels have a number on their sides. That number is track number. When two labels have the same number in two difference frames, it indicates they are the same speckle.

hide **123** **name** are the three buttons used to display and hide the label, track number and speckle name. “hide” button is used to show or hide all the marks on the image, including label, track number and speckle name. “123” is used to only show or hide track number. “name” button is used to only show or hide speckle name.

The size and shape of a speckle label can also be changed through a menu (Figure 7.7).

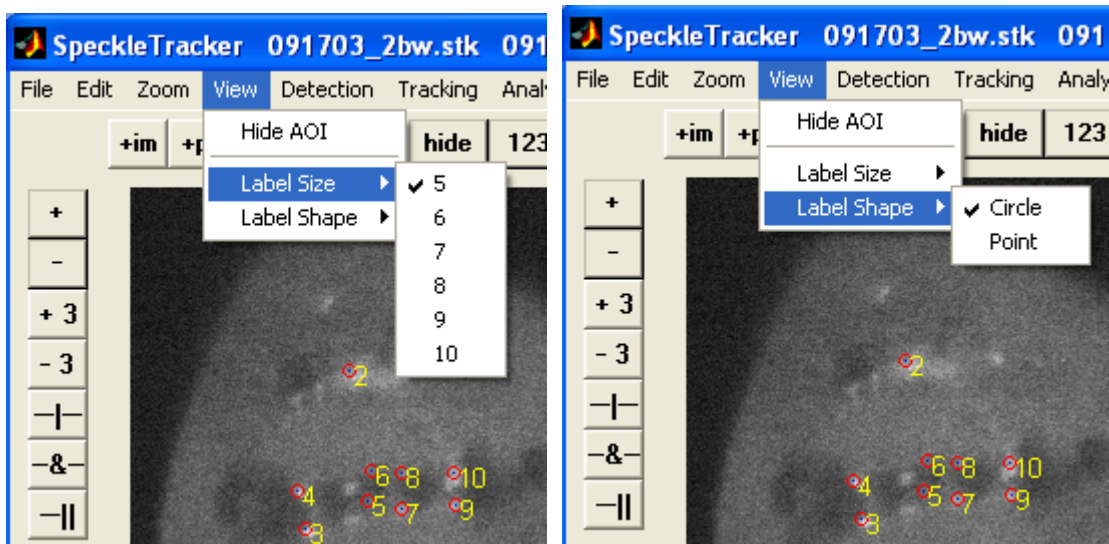


Figure 7.7: Change label

Speckle detection

SpeckleTracker has automatic speckle detection functions. Speckle detector utilizes a special image processing algorithm called mask. Users can adjust its parameters to

achieve maximal detection efficiency. Region of interest (ROI) needs be defined to limit the detection area. Speckles need to be identified before being tracked. Use “detection” menu to select “mask detector” to start the detection. Figure 7.8 shows the “MaskDetector” interface.

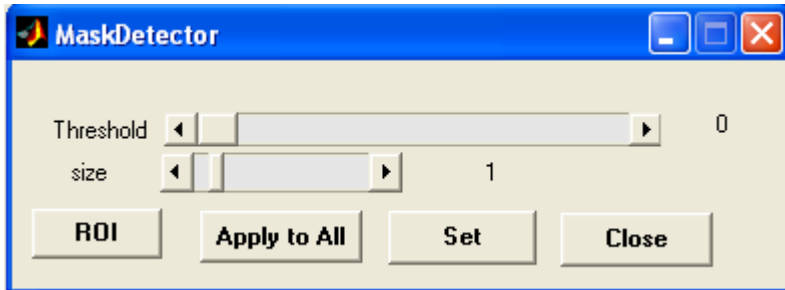


Figure 7.8: Mask detector

The “threshold” bar is used to set the intensity threshold for speckle detection (Chapter 3). The range is from 0 to 1. The higher the threshold, the fewer amounts of speckles will be detected. The “size” bar is used to adjust the variance of the Gaussian mask (Chapter 3).

“ROI” button is used to define a square region of interest. After clicking that button, the cursor will become a cross. Position the cross on the upper left corner of the ROI square, click once. Then position the cross on the lower right corner of the square, click once. The region of interest is therefore defined. If ROI is not used, the detector will address the entire image as default.

To do detection, first define a ROI that includes the minimal area which has all the speckles in interest (Figure 7.9). Then adjust “threshold” and “size” bars to have as many

speckles as you can without introducing too much false detection. Sometimes, including all the speckles you want will bring large amount of false detection. Under this circumstance, raise the threshold a little higher to drop a few speckles and significantly reduce the false detection. Then manually add the missing speckles using the edit functions. If you feel satisfied with the detection, you can apply the detector throughout the rest of the image sequence. Make sure ROI cover all the speckles to be detected for every image before click on “apply to all” to process the rest.

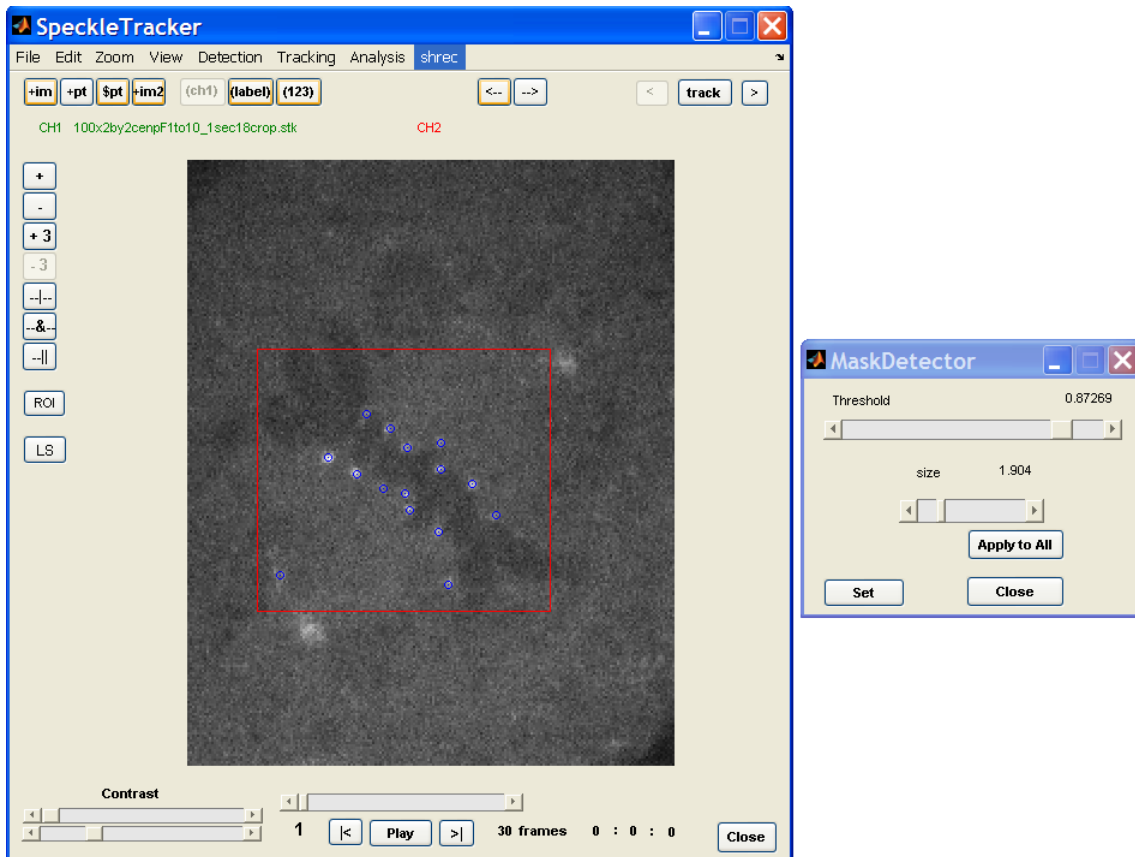


Figure 7.9: Detect kinetochore

Gaussian fitting function

To get accurate coordinates of a speckle, Gaussian fitting is used to find the centroid. From “detection” menu, click “Gaussian Fitting”. Gaussian fitting interface will appear (Figure 7.10).

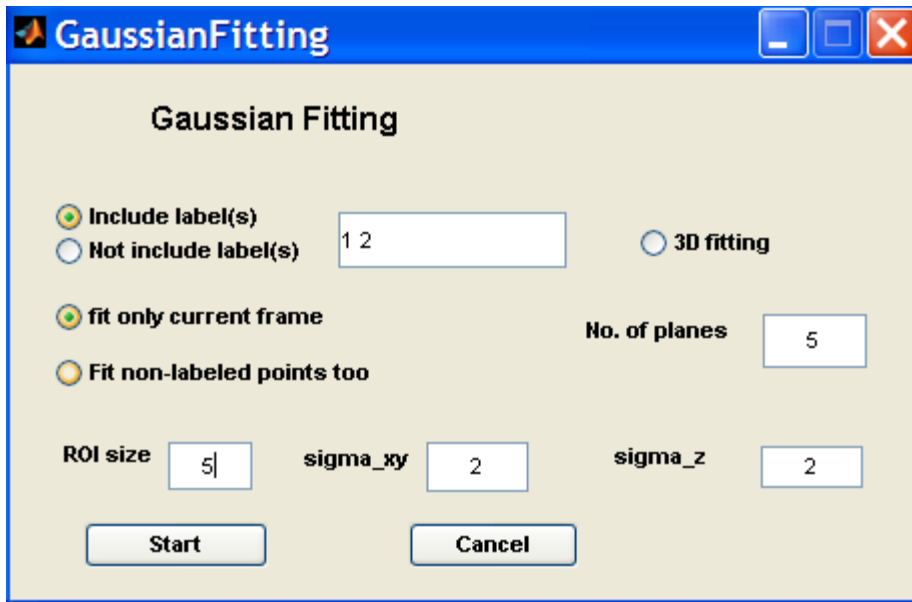


Figure 7.10: Gaussian fitting

It has Gaussian fitting function for both 2D and 3D images. For 3D fitting, check “3D fitting” option (Figure 7.10). User can chose which speckle to fit or not to fit, user can also chose to fit single frame or the whole image sequence. Parameters, such as the size of the fitting area, initial sigma values of Gaussian function, need to be selected. Click “start” button to begin the fitting process.

Speckle tracking

SpeckleTracker tracks the labeled speckle through the image sequence using the nearest neighbor method. Users can modify the tracking results if correction is needed. When all

the speckles you want to study have been detected or labeled, you can start to track them using the automatic tracking function. Click “single particle” from “tracking” menu. Scan through the frames and select the first speckle you are interested in. Click on the label of that speckle, a number “1” will appear on its side. The label also becomes green (indicating being selected). Then click on “track” button. The program will automatically track this speckle throughout the whole sequence. The same speckle in the rest frames will also have a number “1” on its side. The tracking will stop when the last frame being reached or you click on the track button (appearing “stop”) again. You can track the rest of speckles using the same procedure. A number “2” will appear for the second speckle, and so forth.

When all the tracking is finished, uncheck “single particle” from “tracking” menu. Otherwise every time when you select a speckle, the program will think it is in tracking mode and assign a track number to it if it does not already have one.


The automatic tracking does not always follow the right speckle in the next frame due to limit of the tracking method and the errors explained in the tracking chapter. Sometimes manual modification is necessary.


Editing function

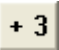
SpeckleTracker provides many easy-to-use editing functions. Users have freedom to add or delete labels to speckles on the image. Track editing is a unique feature of this

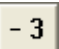
program. Users are able to cut, join, delete or end a track. Those functions make it easy and flexible for users to modify the result of automatic detection and tracking.

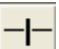
The buttons on the left of the main interface are the editing function buttons (Figure 7.1).

 is the button to add a label to a speckle. After clicking on that button, the cursor will become a cross. Put the cross to the position where you think the centroid of a speckle is. Then click, a label will appear over the speckle.

 is the button to delete the label of a speckle. Click on the button, and the cursor will become a cross. Put it over the label you want to delete and click on it. The label will be deleted.

 is used to add a track number to a label.

 is used to delete a track number from a label. Click it once and then click on the label you want to delete the track number. That entire track is deleted but the label is kept.

 is used to split one track into two tracks. When the automatic tracking gives the wrong result because the track number follows a wrong speckle, use this function to disassociate the track from the wrong speckle. After pressing on this button, click on the label where the wrong track number starts. A new track number will be generated for the rest of the track.

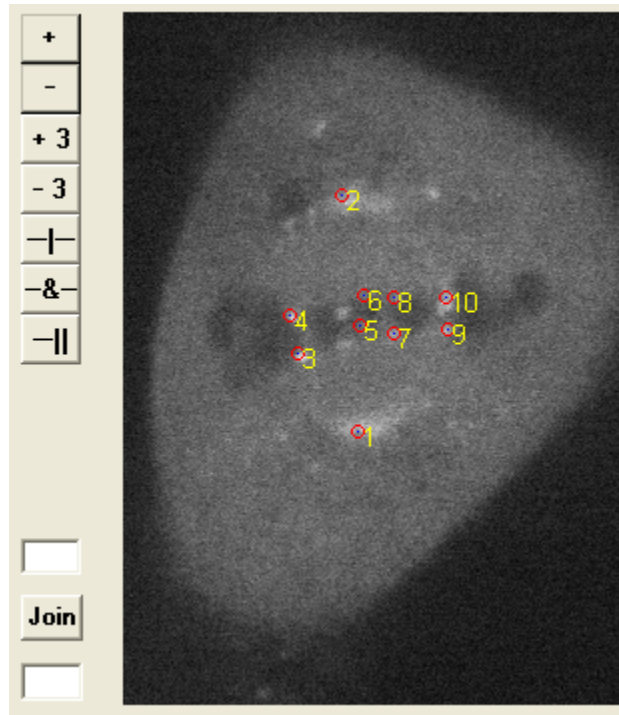


Figure 7.11: Tracking

& is used to connect two tracks. When you find the same speckle has two different track numbers throughout the sequence, use this function to join the two tracks into one. First press this button, click on a label with the first track number, then click on a label with the second track number. The two tracks will become one with the smaller track number of the two. There is another way to do it. Use the “join” button after you input the track numbers into the two boxes nearby.

-|| is used to terminate a track. It is similar to cut track button. The difference is that the rest of track will be deleted.



are the undo and redo buttons. You can also perform undo and redo through “edit” menu.

Save speckle labels

To save the tracking and detection results, click “Save Labels” from “File” menu, or click on “\$pt” button. Also input the scale units (Figure 7.12) before saving to any files.

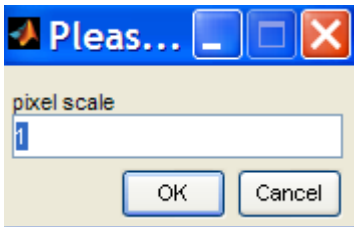


Figure 7.12: Input scale factor

You can save the detection, tracking and editing results to an excel file. Sometimes there are labels without a track number in the image (Figure 7.13). They might be noise, useless speckles or untracked speckles. When saving the data, you will have the options to save those non-track labels. If you are about to save your unfinished work, it is better to save everything into a file. If you already have a complete result, you may want to only save the labels with track numbers.



Figure 7.13: Save labels

Analysis functions

SpeckleTracker can analyze kinetics of kinetochore movement. It can calculate the distances between the kinetochore to the pole, the distance between sister kinetochores and the velocities of kinetochores. Interactive plots are used to assist such relationship study.

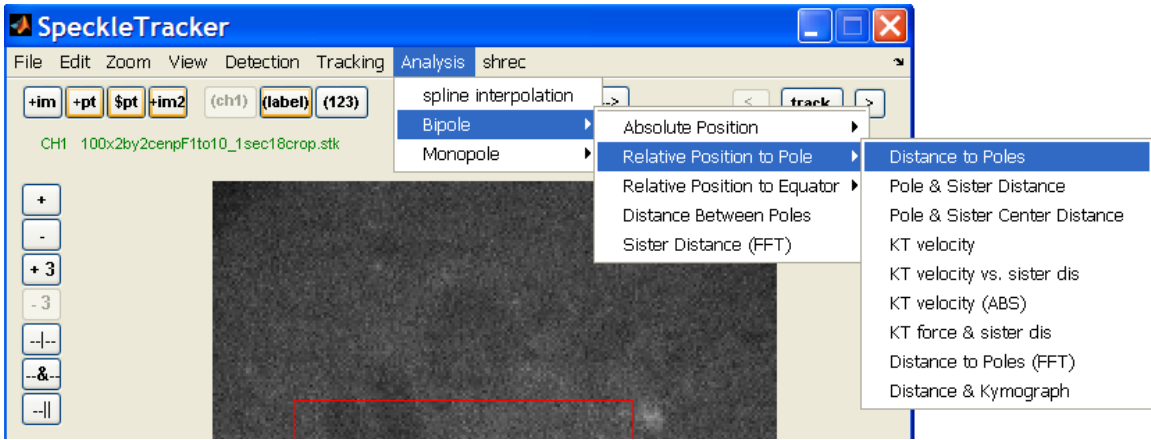


Figure 7.14: Plot kinetochore position

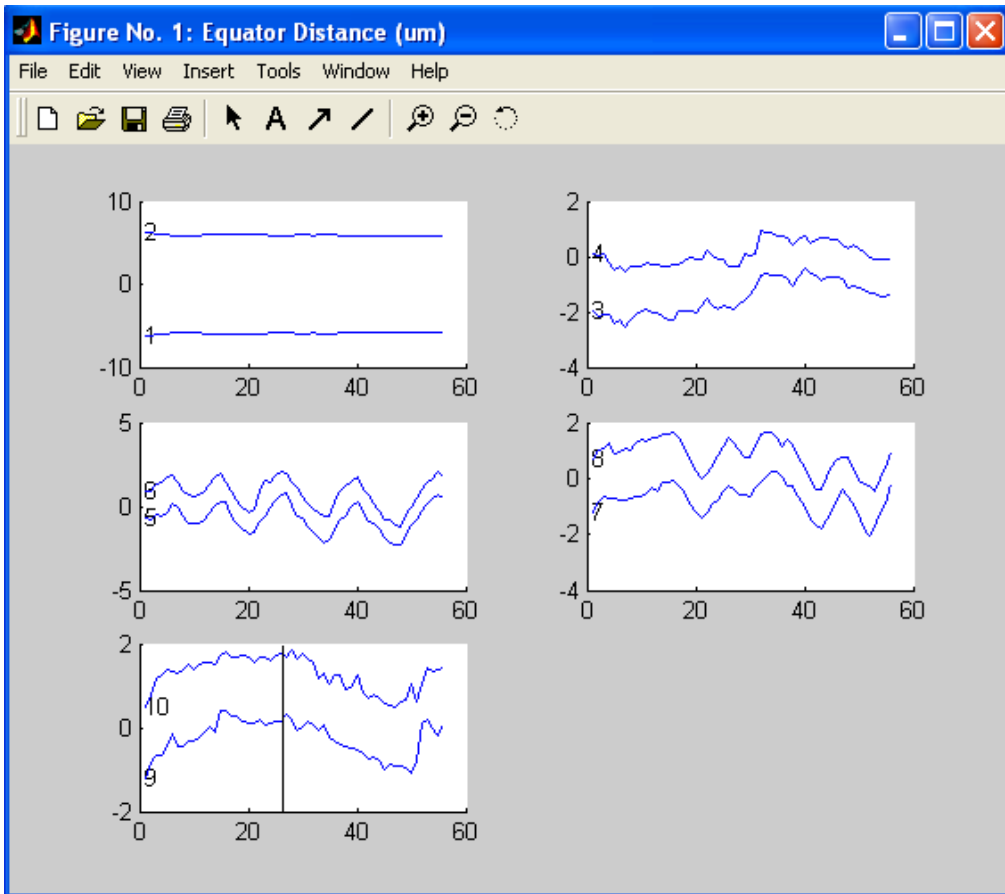


Figure 7.15: Distance between kinetochore and equator

Figure 7.15 shows the distance from kinetochore to equator. Every plot in Figure 7.15 shows a sister kinetochore pair except the first one, which shows the pole positions. The number corresponds to the track number on image. There is a black bar on the bottom plot (Figure 7.14). It can move with the cursor. Clicking on the plot will bring up the image frame corresponding to the position. This is a very convenient method for checking the accuracy of a tracked data point if its position in the distance plots is suspected.

Figure 7.16 shows pole and sister kinetochore distance. The blue and red curves with a number in the beginning show the kinetochore to pole distance for a pair of sister kinetochore. The lower blue curve indicates the sister inner-kinetochore distance. The red dash line is the average sister inner-kinetochore distance.

Oscillation frequency can also be obtained (Chapter 5, Figure 5.3).

Software installation

To run SpeckleTracker program, first copy the whole “SpeckleTracker” directory to the installation directory. Then add path of that directory and its sub directories to MATLAB search path. Type “SpeckleTracker” and hit enter key in command window, the program will start.

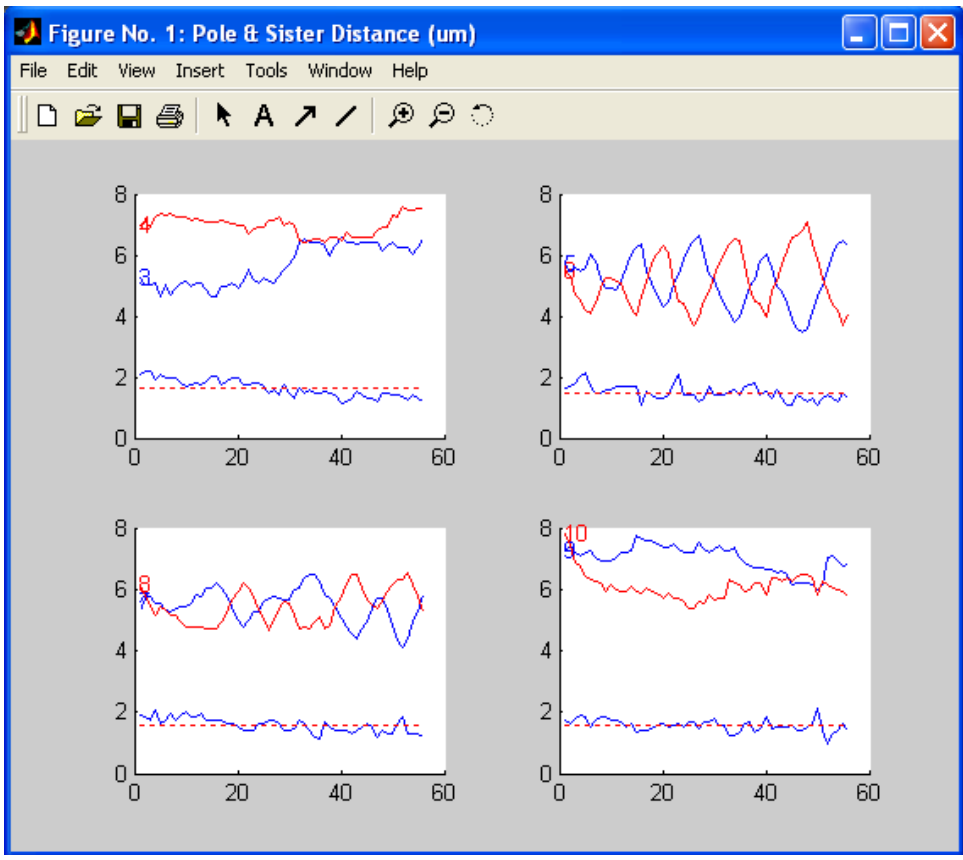


Figure 7.16: Distance between kinetochore and pole

REFERENCES

- Brinkley, B.R., I. Ouspenski, and R.P. Zinkowski. 1992. Structure and molecular organization of the centromere-kinetochore complex. *Trends Cell Biol.* 2:15-21.
- Cameron, L.A., G. Yang, D. Cimini, J.C. Canman, O. Kisurina-Evgenieva, A. Khodjakov, G. Danuser, E.D. Salmon. 2004. Kinesin 5-independent poleward flux of kinetochore microtubules in PtK1 cells. *J Cell Biol.* 173(2):173-9.
- Cheeseman, I.M., T. Hori, T. Fukagawa, and A. Desai. 2008. KNL1 and the CENP-H/I/K Complex Coordinately Direct Kinetochore Assembly in Vertebrates. *Mol Biol Cell.* 19:587-94.
- Churchman, L.S., Z. Okten, R.S. Rock, J.F. Dawson, and J.A. Spudich. 2005. Single molecule high-resolution colocalization of Cy3 and Cy5 attached to macromolecules measures intramolecular distances through time. *Proc Natl Acad Sci U S A.* 102:1419-23.
- Ciferri, C., J. De Luca, S. Monzani, K.J. Ferrari, D. Ristic, C. Wyman, H. Stark, J. Kilmartin, E.D. Salmon, and A. Musacchio. 2005. Architecture of the human ndc80-hec1 complex, a critical constituent of the outer kinetochore. *J Biol Chem.* 280:29088-95.
- Ciferri, C., S. Pasqualato, E. Screpanti, G. Varetto, S. Santaguida, G. Dos Reis, A. Maiolica, J. Polka, J.G. De Luca, P. De Wulf, M. Salek, J. Rappsilber, C.A. Moores, E.D. Salmon, and A. Musacchio. 2008. Implications for kinetochore-microtubule attachment from the structure of an engineered Ndc80 complex. *Cell.* 133:427-39.
- Cimini, D., L.A. Cameron, and E.D. Salmon. 2004. Anaphase spindle mechanics prevent mis-segregation of merotelically oriented chromosomes. *Curr Biol.* 14:2149-55.
- DeLuca, J.G., Y. Dong, P. Hergert, J. Strauss, J.M. Hickey, E.D. Salmon, and B.F. McEwen. 2005. Hec1 and nuf2 are core components of the kinetochore outer plate essential for organizing microtubule attachment sites. *Mol Biol Cell.* 16:519-31.
- DeLuca, J.G., W.E. Gall, C. Ciferri, D. Cimini, A. Musacchio, and E.D. Salmon. 2006. Kinetochore microtubule dynamics and attachment stability are regulated by Hec1. *Cell.* 127:969-82.
- Dong, Y., K.J. Vanden Beldt, X. Meng, A. Khodjakov, and B.F. McEwen. 2007. The outer plate in vertebrate kinetochores is a flexible network with multiple microtubule interactions. *Nat Cell Biol.* 9:516-22.

- Foltz, D.R., Jansen, L.E., Black, B.E., Bailey, A.O., Yates, J.R., 3rd, and Cleveland, D.W. (2006). The human CENP-A centromeric nucleosome-associated complex. *Nat Cell Biol* 8, 458-469.
- Hori, T., Okada, M., Maenaka, K., and Fukagawa, T. (2008). CENP-O Class Proteins Form a Stable Complex and Are Required for Proper Kinetochores Function. *Mol Biol Cell* 19, 843-854.
- Inoue, S., and E.D. Salmon. 1995. Force generation by microtubule assembly/disassembly in mitosis and related movements. *Mol Biol Cell*. 6:1619-40.
- Kim, Y., Heuser, J.E., Waterman, C.M., and Cleveland, D.W. (2008). CENP-E combines a slow, processive motor and a flexible coiled coil to produce an essential motile kinetochore tether. *J Cell Biol* 181, 411-419.
- Kiyomitsu, T., C. Obuse, and M. Yanagida. 2007. Human Blinkin/AF15q14 is required for chromosome alignment and the mitotic checkpoint through direct interaction with Bub1 and BubR1. *Dev Cell*. 13:663-76.
- Maddox, P.S., B. Moree, J.C. Canman, and E.D. Salmon. 2003. Spinning disk confocal microscope system for rapid high-resolution, multimode, fluorescence speckle microscopy and green fluorescent protein imaging in living cells. *Methods Enzymol*. 360:597-617.
- Maiato, H., J. DeLuca, E.D. Salmon, and W.C. Earnshaw. 2004. The dynamic kinetochore-microtubule interface. *J Cell Sci*. 117:5461-77.
- Maiato, H., A. Khodjakov, and C.L. Rieder. 2005. Drosophila CLASP is required for the incorporation of microtubule subunits into fluxing kinetochore fibres. *Nat Cell Biol*. 7:42-7.
- Musacchio, A., and Salmon, E.D. (2007). The spindle-assembly checkpoint in space and time. *Nat Rev Mol Cell Biol* 8, 379-393.
- Okada, M., Cheeseman, I.M., Hori, T., Okawa, K., McLeod, I.X., Yates, J.R., 3rd, Desai, A., and Fukagawa, T. (2006). The CENP-H-I complex is required for the efficient incorporation of newly synthesized CENP-A into centromeres. *Nat Cell Biol* 8, 446-457.
- Politi, V., G. Perini, S. Trazzi, A. Pliss, I. Raska, W.C. Earnshaw, and G. Della Valle. 2002. CENP-C binds the alpha-satellite DNA in vivo at specific centromere domains. *J Cell Sci*. 115:2317-27.
- Rattner, J.B., A. Rao, M.J. Fritzler, D.W. Valencia, and T.J. Yen. 1993. CENP-F is a .ca 400 kDa kinetochore protein that exhibits a cell-cycle dependent localization. *Cell Motil Cytoskeleton*. 26:214-26.

- Rieder, C.L. 1982. The formation, structure, and composition of the mammalian kinetochore and kinetochore fiber. *Int Rev Cytol.* 79:1-58.
- Rusan, N.M., Fagerstrom, C.J., Yvon, A.M., and Wadsworth, P. (2001). Cell cycle-dependent changes in microtubule dynamics in living cells expressing green fluorescent protein-alpha tubulin. *Mol Biol Cell* 12, 971-980.
- Skibbens, R.V., V.P. Skeen, and E.D. Salmon. 1993. Directional instability of kinetochore motility during chromosome congression and segregation in mitotic newt lung cells: a push-pull mechanism. *J Cell Biol.* 122:859-75.
- Thomann, D., Rines, D.R., Sorger, P.K., and Danuser, G. (2002). Automatic fluorescent tag detection in 3D with super-resolution: application to the analysis of chromosome movement. *J Microsc* 208, 49-64.
- Waters, J.C., R.H. Chen, A.W. Murray, and E.D. Salmon. 1998. Localization of Mad2 to kinetochores depends on microtubule attachment, not tension. *J Cell Biol.* 141:1181-91.
- Wei, R.R., P.K. Sorger, and S.C. Harrison. 2005. Molecular organization of the Ndc80 complex, an essential kinetochore component. *Proc Natl Acad Sci U S A.* 102:5363-7.